Published as: *Nature*. 2020 April ; 580(7804): 524–529.

Paracrine orchestration of intestinal tumorigenesis by a mesenchymal niche

Manolis Roulis[1,12,†], **Aimilios Kaklamanos**[2,12], **Marina Schernthanner**[1], **Piotr Bielecki**[1], **Jun Zhao**[1,3,4], **Eleanna Kaffe**[1], **Laura-Sophie Frommelt**[1], **Rihao Qu**[1,3,4], **Marlene S. Knapp**[1], **Ana Henriques**[2], **Niki Chalkidi**[2], **Vasiliki Koliaraki**[2], **Jing Jiao**[9], **J. Richard Brewer**[1], **Maren Bacher**[1], **Holly N. Blackburn**[1], **Xiaoyun Zhao**[6], **Richard M. Breyer**[7,8], **Vassilis Aidinis**[2], **Dhanpat Jain**[4], **Bing Su**[6], **Harvey R. Herschman**[9], **Yuval Kluger**[3,4,5], **George Kollias**[2,10,13,†], **Richard A. Flavell**[1,11,13,†]

[1]Department of Immunobiology, Yale University School of Medicine, New Haven, CT, USA.

[2]Biomedical Sciences Research Center ‘Alexander Fleming’, Vari, Greece.

[3]Program of Computational Biology and Bioinformatics, Yale University, New Haven, CT, USA.

[4]Department of Pathology, Yale University School of Medicine, New Haven, CT, USA.

[5]Applied Mathematics Program, Yale University, New Haven, CT, USA.

[6]Shanghai Institute of Immunology, Department of Microbiology and Immunology, Shanghai Jiao Tong University School of Medicine, Shanghai, People’s Republic of China

[7]Department of Veterans Affairs, Tennessee Valley Health Authority.

[8]Department of Medicine, Vanderbilt University Medical Center, Nashville, TN, USA.

[9]Department of Molecular and Medical Pharmacology, David Geffen School of Medicine, UCLA, Los Angeles, CA, USA.

[10]Department of Physiology, Medical School, National and Kapodistrian University of Athens, Athens, Greece.

[11]Howard Hughes Medical Institute, Yale University School of Medicine, New Haven, CT, USA.

[12]These authors contributed equally: Manolis Roulis, Aimilios Kaklamanos

[13]These authors jointly supervised this work: George Kollias, Richard A. Flavell

† richard.flavell@yale.edu, kollias@fleming.gr, emmanouil.roulis@yale.edu.

Author contributions M.R. conceived and designed the study and wrote the manuscript. M.R. designed, performed and analysed experiments in Figs. 1–4 and Extended Data Figs. 1–10, assisted by M.S., L.-S.F., M.S.K., M.B., H.N.B. and J.R.B.; A.K. performed experiments in Fig. 2 and Extended Data Figs. 3, 9, assisted by V.K., N.C. and A.H. P.B. implemented Drop-seq. J.Z., R.Q. and Y.K. analysed Drop-seq data. E.K. and V.A. implemented HPLC–MS/MS analyses. X.Z. and B.S. performed in situ hybridization, H.R.H. and J.J. contributed *Ptgs2*$^{f/f}$ and *Ptgs2*^{LSL} mice, R.M.B. contributed *Ptger4*$^{f/f}$ mice and D.J. contributed human FFPE tissues. G.K. and R.A.F. supervised all research, participated in the interpretation of results and edited the manuscript.

Competing interests R.A.F. is a scientific advisor to GlaxoSmithKline and a shareholder and consultant for Zai Lab. All other authors declare no competing interests.

Peer review information *Nature* thanks Garret A. FitzGerald, Dominic Grün, Kun-Liang Guan, Don W. Powell, Omer Yilmaz and the other, anonymous, reviewer(s) for their contribution to the peer review of this work.

Abstract

The initiation of an intestinal tumour is a probabilistic process that depends on the competition between mutant and normal epithelial stem cells in crypts[1]. Intestinal stem cells are closely associated with a diverse but poorly characterized network of mesenchymal cell types[2,3]. However, whether the physiological mesenchymal microenvironment of mutant stem cells affects tumour initiation remains unknown. Here we provide in vivo evidence that the mesenchymal niche controls tumour initiation in *trans*. By characterizing the heterogeneity of the intestinal mesenchyme using single-cell RNA-sequencing analysis, we identified a population of rare pericryptal *Ptgs2*-expressing fibroblasts that constitutively process arachidonic acid into highly labile prostaglandin E_2 (PGE_2). Specific ablation of *Ptgs2* in fibroblasts was sufficient to prevent tumour initiation in two different models of sporadic, autochthonous tumorigenesis. Mechanistically, single-cell RNA-sequencing analyses of a mesenchymal niche model showed that fibroblast-derived PGE_2 drives the expansion of a population of Sca-1^+ reserve-like stem cells. These express a strong regenerative/tumorigenic program, driven by the Hippo pathway effector Yap. In vivo, Yap is indispensable for Sca-1^+ cell expansion and early tumour initiation and displays a nuclear localization in both mouse and human adenomas. Using organoid experiments, we identified a molecular mechanism whereby PGE_2 promotes Yap dephosphorylation, nuclear translocation and transcriptional activity by signalling through the receptor Ptger4. Epithelial-specific ablation of *Ptger4* misdirected the regenerative reprogramming of stem cells and prevented Sca-1^+ cell expansion and sporadic tumour initiation in mutant mice, thereby demonstrating the robust paracrine control of tumour-initiating stem cells by PGE_2–Ptger4. Analyses of patient-derived organoids established that PGE_2–PTGER4 also regulates stem cell function in humans. Our study demonstrates that initiation of colorectal cancer is orchestrated by the mesenchymal niche and reveals a mechanism by which rare pericryptal *Ptgs2*-expressing fibroblasts exert paracrine control over tumour-initiating stem cells via the druggable PGE_2–Ptger4–Yap signalling axis.

Mesenchymal cells are localized in tight association with stem cells in crypts, separated from them by a layer of extracellular matrix less than a 1 μm in thickness (Extended Data Fig. 1a, b). To investigate the heterogeneity of intestinal mesenchymal cells and identify specific pathways that could control stem cell dynamics, we performed single-cell RNA-sequencing (RNA-seq) analysis in the mouse intestinal mesenchyme. By sequencing 3,179 non-epithelial, non-immune cells we identified all major mesenchymal cell types of the lamina propria, including vascular and lymphatic endothelial cells, pericytes, smooth muscle cells and glial cells (Fig.1a). Our analyses also revealed the existence of four different fibroblast populations—which we designate F1 to F4—all characterized by expression of *Pdgfra* (Fig. 1b); F1 and F2 cells are *Pdgfra*^{low}, whereas F3 and F4 cells are *Pdgfra*^{high} (Fig. 1b). A similar division of fibroblasts into *PDGFRA* high and low populations was found in a single-cell dataset[3] of the human colonic mesenchyme (Extended Data Fig. 1h). Confocal and two-photon imaging in *Pdgfra*$^{eGFP/+}$-knockin mice[4] confirmed the presence of Pdgfra^{high} and Pdgfra^{low} fibroblasts and revealed a distinct localization of these two populations in the adult intestine (Extended Data Fig. 2a, b). A dichotomous and compartmentalized expression of Pdgfra was observed in the intestinal mesenchyme throughout postnatal development and on embryonic day 15, when Pdgfra^{high} cells are

associated with early villus formation, whereas Pdgfra^{low} cells occupy the rest of the mesenchyme (Extended Data Fig. 2c). Among *Pdgfra*^{low} cells, F1 fibroblasts comprise two subsets (F1a and F1b), both marked by expression of *Cd34* and *Has1* (Fig. 1b). Population F2 expresses *Cd34* and *Fgfr2* and comprises four subsets (F2a–F2d) occupying diverse niches in the intestine, as shown in *Fgfr2*^{mCherry}-knockin mice[5] (Fig. 1b, Extended Data Fig. 2d). Among *Pdgfra*^{high} cells, F3 cells express the Cajal-cell marker *Ano2* whereas F4 cells express *Acta2*, consistent with a myofibroblast phenotype (Fig. 1b). To understand the potential functions of these uncharacterized populations we performed pathway analyses. We observed a robust enrichment of arachidonic acid metabolism genes in F3 (Cajal) cells and in the small population of F2d fibroblasts (Extended Data Fig.1g, Supplementary Table 1), a pathway strongly associated with colorectal cancer[6]. Arachidonic acid is processed by cyclooxygenases to prostanoids, highly bioactive lipid mediators with a very short half-life and an autocrine or paracrine function in tissues[6]. In humans, pharmacological inhibition of cyclooxygenase-2 (Cox-2) prevents both hereditary and sporadic forms of colorectal cancer through an unknown cellular mechanism, but adverse cardiovascular effects currently impede its clinical application[7]. By fractionating normal human colonic tissues we found that expression of the Cox-2-encoding gene *PTGS2* is nearly undetectable in the epithelium but occurs predominantly in stromal cells; the same pattern as observed in the mouse intestine (Extended Data Fig. 1c, d). Our single-cell analyses showed that in the steady-state, mouse intestine *Ptgs2* is predominantly expressed in F3 (Cajal) cells and in the *Pdgfra*^{low}*Fgfr2*$^{+}$*Vcam1*^{high} F2d fibroblasts (cluster 13) (Fig. 1c, Extended Data Fig. 1f). In humans, *PTGS2* is mainly expressed in *PDGFRA*^{low}*FGFR2*$^{+}$*VCAM1*$^{+}$ fibroblasts (cluster 8) and, to a lesser extent, in other fibroblast populations (Extended Data Fig. 1h). Immunostaining of Cox-2 protein in the mouse intestine verified the presence of a Cox-2-expressing fibroblast population in the muscular layer, a location consistent with that of Cajal cells, and a second rare Cox-2-expressing fibroblast population located around part of the crypts, in close proximity to the stem cell zone, suggestive of the F2d fibroblast cluster (Fig. 1d). We named these cells rare pericryptal Ptgs2-expressing fibroblasts (RPPFs). In agreement with their pericryptal location, RPPFs are marked by expression of the laminin subunit A1 (encoded by *Lama1*), a basement membrane protein detected specifically at the mesenchymal–epithelial interface, and also by expression of R-spondin 1 (encoded by *Rspo1*), a stem cell niche factor detected mainly at the crypt base (Fig. 1b, Extended Data Fig. 2e, f).

Given the localization of RPPFs within the stem cell microenvironment, we aimed to understand their role as a potential mesenchymal niche of tumour-initiating stem cells. We used fibroblast-specific *Col6-Cre* mice, which target a substantial fraction of Pdgfra^{+} intestinal fibroblasts, including fibroblasts surrounding the crypts and Cox-2-expressing fibroblasts, as shown by lineage tracing, flow cytometry in reporter mice and quantitative PCR with reverse transcription (RT–qPCR) analyses in Col6-Cre^{+} cells separated by fluorescence-activated cell sorting (FACS) (Extended Data Fig. 3a–c). Specific ablation of Cox-2 in *Col6-Cre*$^{+}$ fibroblasts in *Col6-Cre-Ptgs2*$^{f/f}$ mice (*Ptgs2*$^{\Delta Fibr}$) was efficient and led to a significant reduction of *Ptgs2* expression levels in the whole tissue (Extended Data Fig. 3d, e), thereby confirming that fibroblasts are a predominant source of Cox-2 in the steady-state intestine.

To address the role of RPPFs in the mesenchymal niche in early tumour initiation, we used the $Apc^{Min/+}$ mouse model in which autochthonous intestinal tumours are spontaneously formed by stem cells losing heterozygosity[8]. This model is highly relevant to human cancer, since somatic or germline mutations in the *APC* gene, a negative regulator of Wnt–β-catenin signalling, drive sporadic or hereditary forms, respectively, of intestinal neoplasia. Intestinal stem cell-specific *Apc* ablation is sufficient to drive tumorigenesis[8]. Notably, although adenoma formation in Apc-mutant mice is known to be Cox-2-dependent, the pathway by which this is mediated remains unknown[9,10]. Thus, we generated $Apc^{Min/+}Ptgs2^{\Delta Fibr}$ mice and studied adenoma formation. We found that specific ablation of *Ptgs2* in fibroblasts led to a strong reduction in the number of microadenomas formed in the small intestine at the early stage of 5 weeks (Fig. 2a) and significantly fewer macroscopic tumours formed at 5.5 months (Fig. 2b), along with a milder splenomegaly and a significantly prolonged survival (Extended Data Fig. 3f, g). We observed no difference in tumour size in $Apc^{Min/+}Ptgs2^{\Delta Fibr}$ mice (Extended Data Fig. 3h), which showed that mesenchymal Cox-2 is necessary for tumour initiation but not for tumour growth. To understand how critical Cox-2 expression in the mesenchymal niche is for tumour initiation, compared with other cellular sources of prostanoids, we examined whether selective Cox-2 expression in fibroblasts is sufficient to drive tumour initiation in Apc-mutant mice. For this purpose, we genetically engineered mice in which a loxP-stop-loxP cassette was knocked into the *Ptgs2* gene, thereby preventing its expression ($Ptgs2^{OFF}$) unless excised by Cre-mediated recombination, which reactivates the gene ($Ptgs2^{ON}$) (Extended Data Fig. 3i). By crossing these with *Col6-Cre* mice, we generated mice in which *Ptgs2* is expressed exclusively in fibroblasts ($Ptgs2^{FibrON}$). We found that control $Apc^{Min/+}Ptgs2^{OFF}$ mice developed only a few intestinal tumours, consistently with the phenotype of *Ptgs2*-knockout mice in this model[9]. By contrast, $Apc^{Min/+}Ptgs2^{FibrON}$ mice—in which *Ptgs2* is expressed exclusively in fibroblasts—displayed robust tumorigenesis and developed, on average, 30 adenomas per mouse in the small intestine (Fig. 2c). Thus, Cox-2 in fibroblasts is both necessary and sufficient for tumour initiation in Apc-mutant mice. To further establish the role of Cox-2-expressing fibroblasts in controlling tumorigenesis, we used a model of sporadic colonic tumorigenesis, which is driven by random mutations caused by repeated injections of azoxymethane, a potent mutagenic agent. We found that $Ptgs2^{\Delta Fibr}$ mice displayed a significantly lower incidence of dysplasia and adenoma formation in the colon at 28 weeks of age (Fig. 2d), along with a reduced number—but not reduced size—of adenomas and dysplastic foci per mouse (Extended Data Fig. 3j). These results from two different models demonstrated in vivo that fibroblasts utilize the Cox-2 pathway to provide a tumour initiation-conductive microenvironment for mutated stem cells in the intestine. Thus, we show that resident fibroblasts physiologically control tumorigenesis in *trans*.

To identify which Cox-2-mediated prostanoids are secreted by fibroblasts in the crypt microenvironment in vivo and drive tumour initiation, we performed lipidomic analyses by liquid chromatography–tandem mass spectrometry (HPLC–MS/MS) in the intestine of $Ptgs2^{\Delta Fibr}$ mice. We identified a significant reduction in the relative abundance of PGE_2 and prostaglandin I2 (PGI_2) in the whole tissue (Fig. 2e), consistent with the expression of the respective synthases, Ptges and Ptgis, in fibroblasts (Extended Data Fig. 1g), and a trend for decreased prostaglandin D2 (PGD_2) and prostaglandin F2α ($PGF_{2\alpha}$) abundance. Out of

these prostaglandins, PGE_2 promotes sporadic tumour formation[11,12] but its cellular source, its cellular target and the receptor through which it acts have remained unknown. These are important considerations for therapeutic targeting in light of the adverse effects of Cox-2 inhibition[7]. Since the estimated half-life of PGE_2 in vivo is less than 15 s (ref.[13]), we hypothesized that PGE_2 secreted by RPPFs may diffuse through the thin (less than 1 μm) basal lamina matrix and reach the neighbouring mutant stem cells at a concentration sufficient to signal and drive tumour initiation.

To study the effect of PGE_2 on intestinal stem cell function we cultured crypts in organoid growth media (OGM) supplemented daily with 16,16-dimethyl PGE_2 ($dmPGE_2$), a derivative of PGE_2 with a prolonged half-life. Notably, PGE_2 prevented the formation of budding organoids, leading instead to the development of spheroid-like structures which lack the typical crypt-villus architecture (Extended Data Fig. 4a). This morphology is associated with poor differentiation and increased stemness[14]. We functionally assessed stem cell activity and found that PGE_2-driven spheroids contain more stem cells with full organoid-forming capacity (Extended Data Fig. 4b). PGE_2 signals through four receptors, EP1–EP4 (encoded by *Ptger1–Ptger4*, respectively, all of which are expressed in the mouse intestine (Extended Data Fig. 5a). We found that EP4 is the major PGE_2 receptor expressed in the mouse intestinal epithelium, in stem and progenitor cells and in the normal human colon (Extended Data Fig. 5b–d). We then generated intestinal epithelial cell-specific *Villin-Cre-Ptger4*$^{f/f}$ mice (*Ptger4*$^{\Delta IEC}$) and found that unlike control crypts, crypts from these mice were able to form budding organoids even when $dmPGE_2$ was added to the OGM (Fig. 3a). On the basis of these results, we focused on the specific role of epithelial Ptger4 in tumour initiation.

To model the mesenchymal niche of intestinal stem cells, we developed a 3D organotypic co-culture comprised of primary intestinal fibroblasts and fresh crypts growing in OGM. When co-cultured with fibroblasts, the majority of crypts developed into spheroids rather than organoids (Fig. 3b). Addition of Ptger4 inhibitors or co-culture with *Ptger4*$^{\Delta IEC}$ crypts was sufficient to restore the growth of budding organoids (Fig. 3c, Extended Data Fig. 4c). Thus, organotypic cultures show that fibroblasts control stem cell function via paracrine PGE_2–Ptger4 signalling.

To understand the specific effects of fibroblast-derived PGE_2 on stem cell function and differentiation we performed single-cell RNA-seq in crypt–fibroblast co-cultures in which Ptger4 signalling was either active (Ptger4-ON) or inhibited (Ptger4-OFF) (Fig. 3d). We analysed 2,192 cells out of which 1,585 were epithelial (Extended Data Fig. 4d). By clustering and aligning these cells with signatures of known intestinal epithelial populations[15] (Extended Data Fig. 4e), we observed a markedly different cellular composition between Ptger4-ON and Ptger4-OFF co-cultures (Fig. 3d, e). First, fibroblast-derived PGE_2–Ptger4 signalling prevented the terminal differentiation of enterocytes but not that of goblet or Paneth cells (Fig. 3e, f). Second, it induced a substantial expansion of a non-cycling population displaying an intermediate transcriptional profile between stem and tuft cells (cluster 3) (Fig. 3f–h, Extended Data Fig. 4f). These cells express specific marker genes such as *Ly6a* (which encodes Sca-1), *Clu*, *Msln* and *Il1rn* (Extended Data Fig. 6b). *Clu* is a marker of revival stem cells[16], a quiescent population that functions as reserve stem

cells (RSC)[24], and is induced upon irradiation damage in the intestinal epithelium. We found that the overall transcriptional program of cluster 3 cells is highly similar to that of RSCs (Fig. 3i, Extended Data Fig. 4g). Furthermore, *Ptger4* is expressed in RSCs and is strongly induced following irradiation damage in the regenerative intestinal epithelium (Extended Data Fig. 5e).

To understand the molecular link between PGE_2–Ptger4 and the RSC phenotype, we first tested whether PGE_2 activates the β-catenin pathway as reported in wound-associated epithelial cells[17]. However, we found a strong downregulation of the β-catenin transcriptional program in RSCs compared with cycling stem cells and no overall difference in this pathway between the Ptger4-ON and Ptger4-OFF conditions (Fig. 3j, Extended Data Fig. 4h, k). By contrast, we observed that Ptger4-ON spheroids overexpressed a set of genes reported to be targets of Yap[18] as well as overall overexpression of a Yap transcriptional program[18] (Extended Data Figs. 4k, 6a, b). This effect was validated in independent PGE_2-driven spheroid cultures and confirmed genetically to be mediated by Ptger4 (Extended Data Fig. 6c–e). Yap is a transcriptional effector of Hippo signalling, which is involved in stemness, organ size control, tissue homeostasis, regeneration and cancer[19] and is key for RSC function[16]. Yap is also indispensable for tumorigenesis driven by Apc-deficient stem cells[18,20]. Indeed, we found that a signature of early $Apc^{min/+}$ tumorigenesis correlated with the Yap program (Extended Data Fig. 6f) and both were predominantly expressed in RSCs (Fig. 3k, l and Extended Data Fig. 4i, j).

To directly examine whether Yap mediates fibroblast-driven expansion of RSCs, we isolated crypts from intestinal epithelial cell-specific *Villin-Cre-*$Yap1^{f/f}$ mice ($Yap1^{\Delta IEC}$) and co-cultured them with fibroblasts in OGM. Although $Yap1^{\Delta IEC}$ crypts require epiregulin supplementation to grow[18], fibroblasts supported their growth in the absence of exogenous epiregulin (Extended Data Fig. 7a). Notably, unlike $Yap1^{f/f}$ crypts, $Yap1^{\Delta IEC}$ crypts did not form spheroids in these co-cultures, but instead retained their crypt morphology (Extended Data Fig. 7a). Flow cytometry analyses for the RSC marker Sca-1 showed a robust expansion of Sca-1^+ cells in co-cultures of fibroblasts with $Yap1^{f/f}$ crypts which was prevented in co-cultures with $Yap1^{\Delta IEC}$ crypts (Extended Data Fig. 7b). Collectively, these analyses revealed that fibroblast-derived PGE_2 drives the expansion of an RSC population with a regenerative/tumorigenic program via Ptger4 and Yap.

Next, we examined how PGE_2 activates a Yap transcriptional program in crypts. In contrast to an earlier study using a cancer cell line[21], stimulation of intestinal organoids with PGE_2 did not induce *Yap1* expression at the RNA or at the protein level (Extended Data Fig. 6g, h). In addition, day 3 PGE_2-driven spheroids showed no difference in total Yap protein expression (Extended Data Fig. 6g). Since G-protein-coupled receptor (GPCR) signalling has been suggested to either activate or inhibit the Hippo–Yap signalling pathway[22], and Ptger4 is a GPCR, we hypothesized that PGE_2 may activate Yap in the intestinal epithelium by inhibiting its regulation by the Hippo pathway. Indeed, when we stimulated wild-type organoids with $dmPGE_2$, we observed Yap dephosphorylation at Ser127 within 30–60 min (Extended Data Fig. 6i), suggestive of inhibition of Hippo activity and activation of Yap. This effect was mediated by Ptger4 (Fig. 4a). Furthermore, stimulation of wild-type organoids with $dmPGE_2$ led to nuclear translocation of Yap within 30–60 min (Fig. 4b) and

transcriptional activation of Yap target genes (Extended Data Fig. 6h), which was prevented by a Ptger4 inhibitor (Fig. 4c). PGE_2-stimulation experiments with *Yap1*$^{\Delta IEC}$ organoids or wild-type organoids treated with verteporfin (an inhibitor of the Yap–Tead interaction[23]) demonstrated that the activation of these genes is mediated by Yap (Fig. 4d, Extended Data Fig. 6j). These results establish that PGE_2–Ptger4 signalling inhibits Hippo activity and, consequently, leads to Yap nuclear translocation and induction of a Yap–Tead-dependent gene-expression program in the intestinal crypt.

Epithelial ablation of Ptger4 in *Ptger4*$^{\Delta IEC}$ mice is efficient but does not affect stem cell function and epithelial lineage differentiation in the steady-state intestine, as assessed by single-cell RNA-seq, 5-bromo-2′-deoxyuridine (BrdU)-incorporation experiments and immunostaining for population markers (Extended Data Fig. 8a–f, i). Lineage tracing of *Ptger4*-deficient Lgr5$^+$ stem cells confirmed that Ptger4 is dispensable for the function of normal stem cells at the steady state (Extended Data Fig. 8h). Similar results were obtained in *Ptgs2*$^{\Delta Fibr}$ mice (Extended Data Fig. 3k). To assess the role of PGE_2–Ptger4–Yap in stem cell reprogramming in vivo, we employed an abdominal-irradiation-induced injury model in the context of which slow-cycling RSC populations are mobilized and mediate the epithelial regenerative response[24]. In the absence of Yap, although no phenotype is observed at the steady state, the epithelial response to irradiation is perturbed, causing increased Paneth cell differentiation[18]. We found that exposure of *Ptger4*$^{\Delta IEC}$ mice to 14 Gy of abdominal irradiation led to a pronounced expansion of Paneth cells three days after irradiation (Fig. 4e, f), thereby phenocopying the effect of Yap deficiency. These results functionally validate the critical function of Ptger4 for RSC mobilization in vivo.

In early tumour initiation, we found that Yap displays an increased nuclear localization in microadenomas of five-week-old *Apc*$^{Min/+}$ mice (Fig. 4g). Furthermore, we observed that Sca-1, a Yap target gene and RSC marker, is detected in the mesenchyme but not in the epithelium in the steady-state in wild-type mice. By contrast, however, in the intestine of five-week-old *Apc*$^{Min/+}$ mice, we observed areas of the epithelium in which Sca-1$^+$ epithelial cells were detected as local expansions, whereas Sca-1$^+$ epithelial cells were more widespread in microadenomas. Similar expansion of Sca-1$^+$ cells has been described in regenerative contexts such as the response to irradiation and to helminth infection[25]. Given these data, we examined the role of Yap in the expansion of Sca-1$^+$ cells and in tumour initiation. In five-week-old *Apc*$^{Min/+}$*Yap1*$^{\Delta IEC}$ mice, we found a markedly decreased number of Sca-1$^+$ areas in the epithelium compared with littermate *Apc*$^{Min/+}$*Yap1*$^{f/f}$ controls, as well as an almost completely abrogated formation of microadenomas (Fig. 4i, j). These results show that in early tumour initiation, Yap translocates to the nucleus and drives the expansion of Sca-1$^+$ cells and the formation of microadenomas. Nuclear localization of Yap and epithelial Sca-1 expression were also observed in developed tumours in five-month-old *Apc*$^{Min/+}$ mice (Extended Data Fig. 9a, b). Moreover, mice treated with repeated azoxymethane injections displayed nuclear localization of Yap in tumours and overexpression of the Yap target gene *Clu* (Extended Data Fig. 9c, ,d).

To address whether fibroblast-derived PGE_2 activates the Yap program and drives tumour initiation via epithelial Ptger4, we generated *Apc*$^{Min/+}$*Ptger4*$^{\Delta IEC}$ mice. Given the crucial role of Yap in tumour initiation, we first examined whether Ptger4 mediates the activation of

Yap target genes in these mice. We found that at five weeks of age, *Apc*$^{Min/+}$ mice displayed an increased expression of Yap target genes, but not of *Yap1* itself, compared with normal controls; however, in *Apc*$^{Min/+}$*Ptger4*$^{\Delta IEC}$ littermates, this upregulation of the same Yap targets was abrogated (Extended Data Fig. 9e). Most notably, five-week-old *Apc*$^{Min/+}$*Ptger4*$^{\Delta IEC}$ mice displayed an attenuated expansion of Sca-1^{+} cells in the epithelium compared with their *Apc*$^{Min/+}$*Ptger4*$^{f/f}$ littermates (Fig. 4k). Moreover, *Apc*$^{Min/+}$*Ptger4*$^{\Delta IEC}$ mice developed fewer microadenomas at five weeks of age (Fig. 4l). They also displayed a strong reduction in the number of macroscopic tumours formed at 5.5 months (Fig. 4m), a significantly alleviated splenomegaly (Extended Data Fig. 9f) and—consistent with a role of Ptger4 in tumour initiation rather than tumour growth—no difference in the size of the tumours formed (Extended Data Fig. 9g). These results provide definitive genetic evidence that epithelial Ptger4 is the receptor that mediates the tumorigenic effect of PGE_2 and explain the role of RPPFs as paracrine drivers of tumour initiation.

On the basis of these results, we addressed the role of PGE_2–PTGER4 in the human intestinal stem cell niche. By isolating crypts from normal parts of the colon from three patients and culturing them in OGM we found that PGE_2 drives the formation of spheroid-like structures. This effect was fully prevented by treatment with a PTGER4 inhibitor, thus confirming that PGE_2–PTGER4 also controls stem cell function in the human colonic crypt (Extended Data Fig. 10a). Furthermore, we performed immunostaining for YAP in tissues from 16 patients, including subjects with sporadic adenomas and adenocarcinomas, familial adenomatous polyposis, Lynch syndrome and cancer associated with inflammatory bowel disease (Supplementary Table 3). We observed that YAP displayed a nuclear localization in tumours but not in the neighbouring normal areas of the tissue in all these samples (Extended Data Fig. 10b), supporting its role in tumorigenesis. Of note, both *PTGER4* and *YAP1* genetic loci were recently identified to be genetically associated with colorectal cancer risk in genome-wide associations studies[26], further underlining the relevance of this pathway to human disease.

The results of this study show that PGE_2-secreting RPPFs provide a micro-niche favouring the activation of the pro-tumorigenic Yap program in neighbouring stem cells, thereby driving tumorigenesis in the presence of mutations (Extended Data Fig. 10c). This work establishes in vivo that the formation of intestinal tumours requires the paracrine interaction of mutated stem cells with their native mesenchymal microenvironment.

METHODS

Mice

Ptgs2$^{f/f}$ mice[27] crossed with *Col6-Cre* mice[28], *Rosa26*$^{mT/mG}$ mice[29] and *Apc*$^{Min/+}$ mice[30] were bred in the animal facilities of the BSRC ‘Alexander Fleming’ under specific pathogen-free conditions. *Ptger4*$^{f/f}$ mice[31] and *Yap1*$^{f/f}$ mice[32] crossed with *Villin-Cre* mice[33] and *Apc*$^{Min/+}$ mice[30], wild-type mice used for organoid experiments, *Lgr5-eGFP-IRES-creERT2* mice[34], *Pdgfra*$^{eGFP/+}$ mice[4], as well as *Col6-Cre* mice[28] crossed with *Rosa26*$^{tdTomato/+}$ mice (Ai14)[35] and *Ptgs2* Lox-Stop-Lox-knockin mice (*Ptgs2*^{LSL}; the generation of this mouse strain is described below) were bred in the facilities of the Yale

Animal Resources Center. All these mice were maintained on a C57BL/6J genetic background. *Fgfr2-T2A-H2B-mCherry* mice[5] were maintained in the facilities of the Icahn School of Medicine at Mount Sinai on the 129S4 genetic background. Mice were housed in standard cages, on a 12:12 h day:night cycle and were fed a standard rodent chow. Mice were used for experiments at 8–12 weeks of age unless otherwise indicated. For all experiments, littermate, co-housed and sex-matched mice were used. Both male and female mice were used for experiments. No mice were excluded from the analyses performed. End points used for mice developing tumours were changes in activity or mobility, abnormal posture, decreased food and/or water intake and decreased body temperature. Experiments in BSRC 'Alexander Fleming' were approved by the Institutional Committee of Protocol Evaluation in conjunction with the Veterinary Service Management of the Hellenic Republic Prefecture of Attika according to all current European and national legislation. All animal experimentation at Yale was performed in compliance with Yale Institutional Animal Care and Use Committee protocols.

Generation of *Ptgs2* Lox-stop-Lox-knockin mice (*Ptgs2*^{LSL})

Ptgs2 flox-stop-knockin mice were generated by the University of California, Davis Mouse Biology Program services. JMB8 (C57BL/6N) embryonic stem (ES) cells were targeted with a vector containing a diphtheria toxin A (PGK-DTA) cassette, a 4 kb 5′ arm of homology, two loxP sites within intron 3 of the *Ptgs2* gene flanking a STOP cassette sequence (derived from Addgene plasmid 11584), and a frt-flanked PKG-neomycin cassette and a 5.1 kb 3′ arm of homology. The PKG-neomycin element enabled positive selection in ES cells, while the DTA element enabled negative selection in ES cells. Mice bearing the targeted lox-stop-frt-PGK-neomycin-frt-lox *Ptgs2* allele in the germline were crossed with the B6N(B6J)-Tg(CAG-Flpo)1Afst/Mmucd transgenic mouse (Mutant Mouse Resource and Research Center MMRC_036512-UCD) and the PGK-neomycin cassette was removed and mice bearing a lox-stop-frt-lox *Ptgs2* allele (*Ptgs2*^{LSL}) were obtained (Extended Data Fig. 3i).

Human subjects

Fresh human colon tissue was obtained from the Yale Pathology Archives on the basis of Yale Human Investigation Committee protocols no. 0304025173, which allows retrieval of tissue from surgical pathology that was consented or has been approved for use with waiver of consent. The data were analysed anonymously from preexisting patient databases and are thus exempt from consent by the human studies committee. Patient characteristics (sex, age, diagnosis) are described in the Supplementary Table 3. All tissue segments were obtained from the uninvolved surgical margins of colon resections. The specific part of the colon resected is indicated in the Supplementary Table 3. Ischaemic time of all samples ranged from 1 h to 3 h. All collected samples were kept on ice-cold RPMI medium before processing.

Formalin-fixed paraffin-embedded colorectal tumour tissue was obtained from the Yale Pathology Archives. The data were analysed anonymously from preexisting patient databases and hence exempt from consent by the human studies committee. Patient characteristics (sex, age, diagnosis) are described in the Supplementary Table 3.

Isolation of human intestinal epithelial cells and stromal cells

For the isolation of intestinal epithelial and stromal cells the tissue was cut into 0.5 cm pieces and incubated five times in HBSS containing 0.5 mM EDTA and 1 mM DTT for 15 min, at 4 °C on a rocker. Epithelial cells were released by vigorous shaking and passed through a 70-μm strainer, washed and used for RNA isolation. For stromal cell isolation the tissue pieces were incubated in DMEM containing 10% FBS, 300 U ml^{-1} Collagenase XI (Sigma, C7657), 0.1 mg ml^{-1} Dispase II (Sigma, D4693) and 50 U ml^{-1} DNase II Type V (Sigma, D8764) for 1 h, at 37 °C, 200 rpm. Cells released after vigorous shaking were passed through a 70-μm strainer, treated with ammonium-chloride-potassium red-blood-cell-lysing buffer, washed with 2% sorbitol and then used for RNA isolation.

Human colonic organoid culture

For the isolation of human colonic crypts the tissue was cut into 0.5-cm pieces and incubated six times in PBS containing 5 mM EDTA and 1 mM DTT for 10 min, at 4 °C on a rocker. Epithelial cells and whole crypts were released by vigorous shaking. The fractions enriched for crypts were further processed. Crypts were washed by centrifugation at 100*g*, 50*g* and 30*g* and then used for organoid development in domes made by Matrigel (Corning, 356231) and IntestiCult Organoid Growth Medium (Human) (Stem Cell Technologies, 06010) according to the manufacturer's guidelines. When indicated, 16,16-dimethyl PGE_2 (Cayman, 14750) dissolved in ethanol was added daily at a final concentration of 0.1 μM. Ethanol was used as a vehicle control for the untreated organoids. The ONO-AE3–208 Ptger4 (EP4) inhibitor (Cayman, 14522) dissolved in DMSO was added at a final concentration of 10 μM 1 h before stimulation and DMSO was used as a vehicle control.

Isolation of mouse intestinal epithelial cells and mesenchymal cells

The intestine was dissected, flushed, opened longitudinally and then cut into 1 cm pieces. The tissues were incubated in HBSS containing 1 mM EDTA, 1 mM DTT, 0.2% FBS, 4–5 times, 10 min each, at 37 °C, 200 rpm. Epithelial cells were released by vigorous shaking, passed through a 70 μm strainer, washed and immediately lysed for RNA isolation. After epithelial cell removal, the remaining stromal part of the intestine was lysed for RNA isolation. For Drop-seq analysis or for FACS-sorting of mesenchymal cells the tissues were processed as above and then incubated in DMEM 10% FBS containing Collagenase XI (300 units/ml, Sigma, C7657), Dispase II (0.1 mg/ml, Sigma, D4693) and DNase II Type V (50 units/ml, Sigma, D8764) for 1 h, at 37 °C, 200 rpm. Cells released after vigorous shaking were passed through a 70 μm strainer and washed with 2% sorbitol. Such cell preparations were directly processed by Drop-seq or by flow cytometry as described below.

Mouse intestinal organoid culture and fibroblast/crypt organotypic co-culture

Crypts were isolated from the last three fourths of the small intestine. The intestine was flushed, cut longitudinally and the villi were scraped off with a glass coverslip. The tissue was then cut into 0.5 cm pieces which were incubated in PBS containing 5 mM EDTA, 0.2% FBS for 30 min at 4 °C on a rocker. Crypts were released by vigorous shaking and were passed through a 70 μm strainer. Six fractions were obtained after vigorous shaking and the ones enriched for crypts were further processed. Crypts were washed by centrifugation at

200*g*, 100*g* and 50*g* and then used for organoid development in domes made by Matrigel (Corning, 356231) and IntestiCult Organoid Growth Medium (Stem Cell Technologies, 06005) according to manufacturer's guidelines. When indicated, $dmPGE_2$ (Cayman, 14750) dissolved in ethanol was added daily at a final concentration of 0.1 μM. Ethanol was used as a vehicle control for the untreated organoids. Crypts isolated from $Yap1^{\Delta IEC}$ mice were cultured in IntestiCult Organoid Growth Medium (Stem Cell Technologies, 06005) supplemented with 0.5 μg ml^{-1} recombinant mouse epiregulin (RnD 1068-EP-050) or co-cultured with intestinal fibroblasts in OGM without epiregulin.

For the assessment of stem cell activity, organoids or spheroids were dissociated into single cells by incubation at 37 °C in 0.25% trypsin-EDTA solution (Gibco, 25200056) diluted 1:1 with DMEM without serum. Numbers of live cells were counted after staining with trypan blue. In each experiment, the same number of live single cells per condition (n = 3,000–11,000) were cultured in domes made by Matrigel (Corning, 356231) and OGM.

Intestinal organoids were stimulated with $dmPGE_2$ at a final concentration of 0.1 μM. Ethanol was used as a vehicle control. The ONO-AE3–208 Ptger4 (EP4) inhibitor (Cayman, 14522) dissolved in DMSO was added at a final concentration of 10 μM 1 h before stimulation. Verteporfin (Cayman, 17334) dissolved in DMSO was added at a final concentration of 1 μM 1 h before stimulation. DMSO was used as a vehicle control for ONO-AE3–208 and Verteporfin.

Fibroblasts were isolated from the small intestine of mice. The intestine was dissected, flushed, opened longitudinally and then cut into 1-cm pieces. The tissues were incubated in HBSS containing 1 mM EDTA, 1 mM DTT and 0.2% FBS 4–5 times for 10 min each, at 37 °C, 200 rpm. Epithelial cells were released by vigorous shaking. Then, the tissues were incubated in DMEM 10% FBS containing Collagenase XI (300 U ml^{-1}, Sigma, C7657), Dispase II (0.1 mg ml^{-1}, Sigma, D4693) and DNase II Type V (50 U ml^{-1}, Sigma, D8764) for 1 h, at 37 °C, 200 rpm. Cells released after vigorous shaking were passed through a 70-μm strainer, washed and cultured in DMEM with 10% FBS. For co-culture experiments 2×10^4 fibroblasts were seeded in 48-well plates overnight. Freshly isolated crypts (n = 500) were suspended in 1:1 Matrigel (Corning, 356231) and OGM and added as an overlay on the fibroblasts. Crypts and fibroblasts were co-cultured with OGM. When indicated, the ONO-AE3–208 Ptger4 (EP4) inhibitor dissolved in DMSO was added to the co-cultures every second day at a final concentration of 10 μM. DMSO was used as a vehicle control for the untreated co-cultures.

Quantitative real-time PCR

RNA was isolated with the TRIzol reagent (Thermo Fisher, 15596026) followed by DNase I treatment (Roche, 04716728001) or with the QIAGEN RNA isolation RNeasy plus Mini Kit (QIAGEN, 74134) according to the manufacturer's instructions. Reverse transcription was performed with the Maxima H Minus Reverse Transcriptase (Thermo Fischer, EP0751). RT–qPCR analyses were performed using iTaq Fast SYBR Green Supermix (Bio-Rad, 1725100) and a CFX96 Touch Real-Time PCR Detection System (Bio-Rad). Data were acquired and analysed with the CFX Manager software (Bio-Rad). Gene expression relative to a control sample was calculated with the RelQuant software (Bio-Rad Laboratories) by normalizing to

B2m expression. Where indicated, relative expression (RE) to *B2m* was calculated as RE = $2^{-\Delta Ct}$. Primers used for human were *B2M*-F: ATGAGTATGCCTGCCGTGTG, *B2M*-R: CCAAATGCGGCATCTTCAAAC, *PTGS2*-F: TGTTGAAAAGTAGTTCTGGG, *PTGS2*-R: AAGCAGGCTAATACTGATAGG. Primers for mouse were *B2m*-F: TTCTGGTGCTTGTCTCACTGA, *B2m*-R: CAGTATGTTCGGCTTCCCATTC, *Ptgs2*: QT00165347 (QIAGEN) and *Ptgs2*-F: TCCAACCTCTCCTACTACACCAG, *Ptgs2*-R: GGGTCAGGGATGAACTCTCTC, *Ptger1*-F: AAGTTTTGGATTCACTTCCC, *Ptger1*-R: GAAGGTGTTGAGATTCTTGG, *Ptger2*-F: CTTGCCTTTCACAATCTTTG, *Ptger2*-R: ACCCAAGGGTCAATTATAGAG, *Ptger3*-F: CGCCGCTATTGATAATGATG, *Ptger3*-R: TTCTTAGCAGCAGATAAACC, *Ptger4*-F: GTGCGGAGATCCAGATGGTC, *Ptger4*-R: TCACCACGTTTGGCTGATATAAC, *Ly6a*-F: GAAAGAGCTCAGGGACTGGAGTGTT, *Ly6a*-R: TTAGGAGGGCAGATGGGTAAGCAA, *Clu*-F: GCTGCTGATCTGGGACAATG, *Clu*-R: ACCTACTCCCTTGAGTGGACA, *Il1rn*-F: GCTCATTGCTGGGTACTTACAA, *Il1rn*-R: CCAGACTTGGCACAAGACAGG, *Cxcl16*-F: CCTTGTCTCTTGCGTTCTTCC, *Cxcl16*-R: TCCAAAGTACCCTGCGGTATC, *Msln*-F: CTTAGTCTTGGGTGGATA, *Msln*-R: TCTTCTGTCTTACAGCCA, *Yap1*-F: GATGTCTCAGGAATTGAGAAC and *Yap1*-R: CTGTATCCATTTCATCCACAC.

Western blot

Total protein was extracted with RIPA lysis buffer. Nuclear and cytoplasmic fractions were extracted with NE-PER Nuclear and Cytoplasmic Extraction Reagents (Thermo Fischer, 78833). Protease inhibitors (Thermo Fischer, 87786) and phosphatase inhibitors (Thermo Fischer, 78420) were added. Antibodies against pYAP (Ser127) (D9W2I) (Cell Signaling, 13008), YAP (D8H1X) (Cell Signaling, 14074) and TBP (D5C9H) (Cell Signaling, 44059) were used at a 1:1,000 dilution in 5% BSA, overnight. Antibodies against β-actin (clone C4, Santa Cruz sc-47778) were used at a 1:2,000 dilution in 5% BSA for 2 h at room temperature.

Immunofluorescence and imaging

Two-photon microscopy was performed with a LaVision TriM Scope II (LaVision Biotec) microscope equipped with a Chameleon Vision II (Coherent) two-photon laser in the In Vivo Imaging Facility of Yale School of Medicine. Fresh whole-mount specimens of the small intestine and the colon of a *Pdgfra*$^{eGFP/+}$ mouse[4] were prepared and analysed immediately after mice were euthanized.

Confocal imaging was performed with a Nikon-Ti microscope combined with UltraVox spinning disk (PerkinElmer) and data were analysed by using the Volocity software (PerkinElmer). Rosa26–tdTomato, Pdgfra–eGFP and Fgfr2–mCherry were detected by direct fluorescence. The tissues were dissected, fixed in 4% paraformaldehyde for 4 h at 4 °C, followed by incubation in 30% sucrose/PBS overnight at 4 °C. Tissue samples were frozen in OCT (Tissue-Tek) on dry ice and kept at −80 °C until sectioning. Sections 10 μm thick were prepared with a cryostat (Leica). After washing with PBS, sections were mounted with Fluoroshield histology medium containing DAPI (Sigma, F6057). For Lgr5–eGFP and vimentin immunostaining, the terminal ileum of a *Lgr5-eGFP-IRES-creERT2* mouse[34], was dissected, frozen and processed as above. The staining was performed with an Alexa Fuor

488-conjugated rabbit polyclonal GFP antibody at 1:200 (Thermo Fisher, A-21311) and an Alexa Fuor 647-conjugated rabbit monoclonal vimentin antibody at 1:200 (Cell Signaling, 9856), overnight at 4 °C. Sca-1 immunostaining was performed in frozen tissue sections processed as above and stained with a rat monoclonal Alexa Fuor 647 antibody (E13–161.7, Biolegend 122517, 1:400) overnight at 4 °C. The number of Sca-1^+ areas was quantified in sections of small intestine prepared with the Swiss-roll technique and an EVOS FL Auto 2 Imaging System (Thermo).

Formalin-fixed paraffin-embedded tissue sections were deparaffinised, washed and antigen retrieval was performed by microwave heating in citrate buffer. For Cox-2 immunostaining an anti-COX2 rabbit polyclonal primary antibody was used (Cayman, 160126) at a 1:150 dilution, overnight at 4 °C with an anti-rabbit Alexa Fuor 488 secondary antibody at a 1:1,000 dilution, for 2 h at room temperature. Immunostaining for epithelial lineage markers was performed with conjugated antibodies against lysozyme (FITC-conjugated rabbit polyclonal, DAKO EC 3.2.1.17, 1:100) and Dclk1 (Alexa Fuor 647 rabbit monoclonal, EPR6085, Abcam ab202755, 1:400) and primary antibodies against chromogranin-A (rabbit polyclonal, Abcam ab15160, 1:300) and Olfm4 (rabbit monoclonal, D6Y5A, Cell Signaling 39141, 1:300) followed by an anti-rabbit Alexa Fuor 488 secondary antibody as above. Immunostaining for Yap was performed with a rabbit monoclonal primary antibody (D8H1X, Cell Signaling 14074, 1:50, overnight at 4 °C), a goat anti-rabbit biotinylated IgG secondary antibody (Vector, 1:750) and Streptavidin–Alexa Fuor 488 (1:800). Colocalization of Yap–Alexa Fuor 488 and DAPI was detected with the colocalization mode of Volocity software (PerkinElmer). Immunostaining for laminin A1 was performed with a rat monoclonal antibody (AL-4, R&D MAB4656, 1:50) overnight at 4 °C and an anti-rat Alexa Fuor 594 secondary antibody at a 1:1,500 dilution, for 1 h at room temperature. The numbers of positive cells for each epithelial marker per well-oriented crypt or crypt-villus unit were quantified in a blinded fashion.

BrdU

Administration of BrdU (Sigma) was performed intraperitoneally at a dose of 100 μg per g of body weight 2 h before mice were euthanized. BrdU immunohistochemistry was performed in sections of formalin-fixed paraffin-embedded tissues with the BrdU In-Situ Detection Kit (BD Pharmingen). The sections were counterstained with haematoxylin and analysed with a Leica DMI6000B microscope equipped with the Leica Application Suite LAS v.2.7 software. The number of $BrdU^+$ cells per well-oriented crypt was quantified in a blinded fashion.

Alkaline phosphatase

Alkaline phosphatase activity was detected in deparaffinized sections with the Vector Red Alkaline Phosphatase Substrate Kit (Vector, SK-5100) in 200 mM Tris-HCl, pH 8.5 according to the manufacturer’s instructions. The sections were counterstained with haematoxylin and mounted with DPX or with Cytoseal Xyl (Thermo).

In situ hybridization

In situ hybridization was performed using the C Multiplex Fluorescent Detection Kit v.2 (ACD Bio) according to the manufacturer's instructions. The colons of eight-week-old wild-type mice were excised, rolled up and immediately frozen in liquid nitrogen before embedding in Tissue-Tek OCT compound (Sakura Finetek). Sections with a thickness of 15 μm were prepared for RNAscope analysis using a mouse *Rspo1* probe (ACD Bio 401991), a mouse *Ppib* positive control (ACD Bio 313911) and the bacterial *DapB* probe as a negative control (ACD Bio 310043). DAPI was used as a nuclear counterstain.

Evaluation of tumorigenesis in $Apc^{Min/+}$ mice

Early tumorigenesis in $Apc^{Min/+}$ mice was examined at the age of five weeks. The entire small intestine was collected and fixed in 10% neutral-buffered formalin solution as a Swiss roll. H&E-stained paraffin sections were examined with a Nikon Eclipse E800 microscope or a Leica DMI6000 B microscope. The number of microadenomas was quantified in sections stained for β-catenin (Fig. 2) or BrdU (Fig. 4). At the age of 5.5 months, tumorigenesis in $Apc^{Min/+}$ mice was evaluated in the small intestine and the colon. The small intestine was partitioned into three parts of equal length (duodenum, jejunum and ileum). The tissues were opened longitudinally and the number of macroscopic tumours was quantified. The opened small intestine was rolled, fixed in formalin and H&E-stained paraffin sections were obtained. Pictures of all adenomas detected per section were obtained and their maximal diameter was measured by using the ImageJ software or the Leica Application Suite LAS v.2.7. All analyses were blinded to mouse genotype.

Azoxymethane-induced colon tumorigenesis

Mice were injected intraperitoneally with 10 mg kg^{-1} of azoxymethane (Sigma, A5486) once per week for 10 weeks starting at the age of 6 weeks. Mice were euthanized at the age of 28 weeks. Dysplasia development and adenoma formation were evaluated in H&E-stained paraffin sections of the colon. RNA was extracted from formalin-fixed, paraffin-embedded tissues with the RecoverAll Total Nucleic Acid Isolation Kit (Thermofisher, AM1975).

Prostanoid analysis by HPLC–MS/MS

Prostanoids were extracted with acetone followed by liquid/liquid extraction as previously described[36], with some modifications. In brief, 10–50 mg of the ileum was homogenized in 500 μl PBS spiked with 100 μM butylated hydroxytoluene on ice. PGE_2-d4 (Cayman, no. 314010) and PGD_2-d4 (Cayman, no. 312010) were used as internal controls in each sample from the beginning of the extraction procedure at a final concentration of 10 ng ml^{-1}. The samples were deproteinized with acetone. After mixing for 4 min and centrifugation at 2,000*g* for 10 min at 4 °C, the samples were transferred to clean 15-ml glass tubes, mixed with 800 μl hexane for 30 s and centrifuged for 10 min at 2,000*g* at 4 °C. The lower phase was acidified to pH 3.5 with formic acid and then mixed with chloroform. After mixing for 30 s and centrifugation for 10 min at 2,000*g* at 4 °C, the lower chloroform phase was evaporated to dryness under a stream of nitrogen and redissolved in 50 μl of methanol. HPLC–MS/MS analysis was performed using a modification of a method previously described[37]. From each sample a volume of 5 μl was injected into a Gemini 5 μm C18 110

Å, 100 × 2 mm HPLC column (Phenomenex, 00D-4435-B0) coupled with an Agilent 6490 QQQ Triple Quadrupole mass spectrometer with electrospray ionization in negative mode (Yale West Campus Analytical Core). The flow rate was 0.2 ml min^{-1} and the column was maintained at ambient temperature. The analysis was performed using an acetonitrile-based gradient system mixing two solvents: solvent A was acetonitrile/water/glacial acetic acid, 45/55/0.02 (v/v/v); solvent B was acetonitrile/water/glacial acetic acid, 90/10/0.02 (v/v/v). The analytes were separated using the following gradient: 0.0–8.0 min, 0% solvent B; 8.0–8.1 min, 0 to 50% solvent B; 8.0–12.0 min 50% solvent B; 12.0–12.1 min, 50 to 70% solvent B; 12.1–20.0 min 70% solvent B; 20.0–20.1 min, 70 to 0% solvent B; 20.1–30.0 min 0% solvent B. The capillary voltage was set at 3,500 V, source temperature at 120 °C, desolvation temperature at 360 °C and cone voltage at 35 V. The detection of prostanoids was based on the multiple reaction monitoring (MRM) method. The transition of precursor masses to specific fragments was monitored using a collision energy of 25–30 eV. PGE_2 and PGD_2 which have a similar MRM mass transition (m/z 351 → 271) and PGE_2-d4/PGD_2-d4 which also have similar MRM mass transition (m/z 355 → 275) were distinguished on the basis of their different elution time from the HPLC column. The MRM mass transition for PGF_{2a} was m/z 353 → 193 and for PGI_2 was m/z 351 → 215. The data were analysed with the Agilent MassHunter Workstation software, v.B.07.00. For each mass transition the area under the curve was normalized with that of the corresponding internal labelled control and a relative abundance was calculated. The relative abundances calculated were normalized based on the weight of the tissue sample. PGD_2-d4 was used as a control for PGD_2 and its metabolites. PGE_2-d4 was used as a control for the rest of the prostanoids.

Single-cell RNA sequencing and data analysis

Single-cell RNA-seq was performed with the Drop-seq protocol as described previously[38,39] with minor modifications. Drop-seq analysis of mesenchymal/lamina propria cells isolated from the middle and distal colon of wild type mice was performed in two biological replicates. For each biological replicate, the colons of $n = 2$ mice were pooled. The vast majority of intestinal epithelial cells were depleted by EDTA treatment as described above. $N = 5$ Drop-seq collections were processed in total, two from the first biological replicate and three from the second (Extended Data Fig. 1e). Drop-seq analysis of Ptger4-OFF and Ptger4-ON crypt/fibroblast co-cultures was performed on day 4 of the protocol in one pool of six Ptger4-ON co-cultures and one pool of six Ptger4-OFF co-cultures with one Drop-seq collection per pool. For Drop-seq analysis of crypts, epithelial cells isolated from the small intestine of $Ptger4^{f/f}$ and $Ptger4^{\Delta IEC}$ mice, tissues from $n = 2$ mice per genotype were independently processed as biological replicates. A total of three Drop-seq collections were processed for each genotype, two from the first biological replicate and one from the second (,Extended Data Fig. 8c).

The cells were diluted to a concentration of 100 cells per μl and 1-ml aliquots were used as input for each collection of the Drop-seq protocol[38,39]. The beads were purchased from ChemGenes (no. Macosko201110) and the polydimethylsiloxane co-flow microfluidic droplet generation device was generated by Nanoshift. Samples were processed for cDNA amplification within ~15 min of collection. Populations of 5,000 beads (~150 cells) were separately amplified for 15 cycles of PCR and pairs of PCR products were co-purified by the

addition of 0.6× AMPure XP beads (Agencourt). Libraries were prepared and tagmented by Nextera XT using 1,000 pg of cDNA input, the custom primer P5_TSO_Hybrid[38] and Nextera XT primers N701-N705 (Illumina). Libraries from intestinal mesenchymal cells and crypt epithelial cells were sequenced on the Illumina HiSeq platform (paired end, 2 × 150 bp) and libraries from crypt–fibroblast co-cultures on the Illumina NextSeq 500 platform (paired end, read 1 20 bp; read 2 60 bp), using a Read1CustomSeqB[38] primer for read 1.

Single-cell RNA-seq data were processed as described[38] to generate a digital expression matrix with transcript count data. This matrix was filtered retaining cells with more than 1,000 transcripts and less than 10% mitochondria transcripts. We then log transformed each entry of the matrix by computing log(TPM/100 + 1), where TPM is transcripts per million (meaning that the sum of all gene levels is equal 1,000,000). After normalization, we used adaptively thresholded low rank approximation (ALRA)[40] to impute the matrix and fill in the technical dropped-out values. Subsequently, to visualize the cell subpopulations in two dimensions, we applied principal component analysis followed by *t*-SNE[41], a nonlinear dimension reduction method, to the log-transformed data. DBSCAN[42] and graph-based clustering (Seurat, Satija lab) were then used to generate clusters that were overlaid on the *t*-SNE coordinates to investigate cell subpopulations. Marker genes for each cluster of cells were identified using the Wilcoxon test with Seurat. Pathway enrichment analysis was performed by GSVA[43] and *P* values were calculated with the moderated *t*-test implemented in the Limma R package. For the adjusted *P* values the false discovery rate (Benjamini–Hochberg) correction method was used.

In the fibroblast–crypt co-culture, single-cell RNA-seq experiment, epithelial cells were distinguished from fibroblasts and selected on the basis of unbiased clustering and known marker genes as shown in the Extended Data Fig. 4d. Cell-cycle analysis was adapted from Seurat. First, a score was calculated for each cell on the basis of the expression of G2M and S phase markers. Then, a discrete classification of cell cycle was assigned to each cell by comparing its G2M and S scores. Cells expressing neither were classified into the G1 group because they are less likely to be cycling.

A metagene score was assigned on the basis of publicly available bulk and single-cell RNA-seq datasets. For each of these datasets we selected significantly differentially expressed genes and constructed a metagene defined as weighted average of the log-transformed expression of these differentially expressed genes with weights equal to the log fold ratio of these genes in the respective dataset. More specifically, if we assume we have a metagene M that contains m genes: $\{\text{gene}_1, \text{gene}_2, \ldots, \text{gene}_m\}$ and each gene i has log fold change log FC_i in the data we use for the signature of interest, and each gene i has an expression value of $x_{\text{gene } i}$ in a given cell in our dataset, then the score for M in this specific cell is calculated as:

$$S_M = \sum_{i=1}^{m} x_{\text{gene } i} \times \log\text{FC}_i$$

Each cell from our single-cell dataset was characterized by a score associated with each of the metagenes. The extent of differential behaviour between distributions of the total cell populations of two different conditions (Ptger4-ON vs Ptger4-OFF cells) was assessed for each metagene using the Kolmogorov–Smirnov test. We built metagenes for stem cells, enterocytes, Paneth cells, goblet cells, enteroendocrine cells and tuft cells by using lists of population-specific genes based upon plate single-cell RNA-seq data from the mouse intestinal epithelium[15]. We also built the following metagenes: (1) a β-catenin program metagene based on bulk RNA-seq data from organoids bearing a murine stabilized mutant *Ctnnb1*^{stab} transgene and normal organoids (GSE93947), (2) A Yap program metagene based on bulk RNA-seq data from Yap-overexpressing and normal crypts isolated from doxycycline-treated and untreated *YapTg* inducible transgenic mice respectively (GSE66567)[18], (3) An early *Apc*$^{min/+}$ tumorigenesis program metagene based on microarray gene-expression data from the nonpolypotic sections of terminal ileum from *Apc*$^{min/+}$ and wild-type mice (GSE49970).

Single-cell RNA-seq data of the healthy human colonic mesenchyme[3] were obtained from GSE114374. Single-cell RNA-seq data of regenerating intestinal crypts[16] were obtained from GSE117783. These datasets were processed by ALRA and the subsequent steps as above.

Abdominal irradiation of mice

For abdominal X-ray irradiation an X-RAD 320 Biological Irradiator (Precision X-ray) was used. Mice were anaesthetized and irradiated individually. 15 mm-thick lead was used for head, limb and tail shielding. Mice were treated at a distance of 50 cm from the radiation source with 320 kV, 12.5 mA X-rays, using a filter consisting of 2.0 mm Al. The mouse abdomen was centred between a 55 mm × 65 mm target window outlined by an adjustable collimator. The dose rate was measured with an ionization chamber by members of the Radiation Safety Division at Yale University. The abdominal dose rate was 235 cGy min^{-1}. Average dose to shielded areas was 3.54 cGy min^{-1}.

Flow cytometry and sorting

Freshly isolated stromal cells from *Col6-Cre-Rosa26*$^{tdTomato/+}$ mice were stained with monoclonal antibodies against CD45 (Biolegend) and used for FACS sorting. FACS sorting was performed at the Yale Flow Cytometry Facility with a BD FACSAria II sorter equipped with FACSDiva 7 software. Freshly isolated stromal cells from *Col6-Cre-Rosa26*$^{mT/mG}$*Ptgs2*$^{f/f}$ mice were sorted on the basis of their GFP and tdTomato fluorescent protein expression with a BD FACSAria III sorter (BD) equipped with FACSDiva software at the Flow Cytometry Facility of BSRC Fleming. Single-cell suspensions from organoid cultures and co-cultures were obtained as described above, stained with monoclonal antibodies against Cd24 (Clone M1/69, Biolegend) and Sca-1 (Clone D7, Biolegend) and analysed at the Yale Flow Cytometry Facility with a BD LSRII cytometer equipped with FACSDiva software. Data analysis was performed with the FlowJo software.

Statistical analysis

Statistical analyses were performed with GraphPad Prism 7.01. Normality was tested with the Shapiro–Wilk W test. For $W < 0.05$, differences in means were tested for statistical significance with two-tailed Mann–Whitney test or Kruskal–Wallis test. For $W > 0.05$, variances were compared by F test and if similar (F test, $P > 0.05$), unpaired two-tailed Student's t-test or one-way ANOVA was applied, otherwise (F test, $P < 0.05$) unpaired two-tailed Welch's t-test was applied. For paired comparisons, statistical significance was tested with paired t-test for $W > 0.05$ or with Wilcoxon matched-pairs signed-rank test for $W < 0.05$. P values <0.05 were considered as statistically significant. Survival curves were compared by the log-rank test using GraphPad Prism 7.01.

Reporting summary

Further information on research design is available in the Nature Research Reporting Summary linked to this paper.

Data availability

All data that support the findings of this study are available within the paper and its Supplementary Information files. All Drop-seq data that support the findings of this study have been deposited in the Gene Expression Omnibus (GEO) repository with the accession code GSE142431.

Code availability

The code used for single-cell RNA-seq data analysis is available in GitHub (https://github.com/KlugerLab/Scripts_Roulis_et_al_2020).

Extended Data

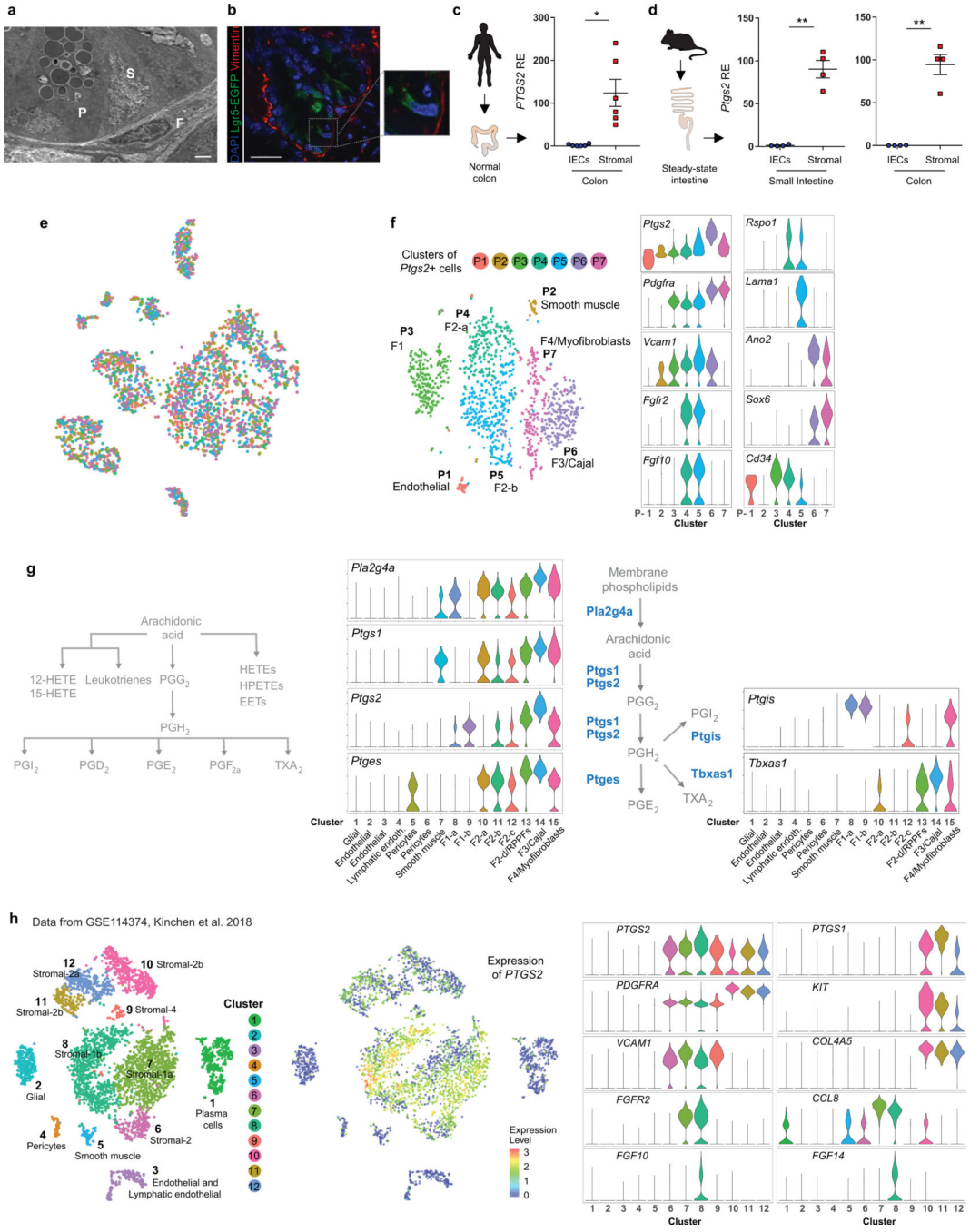

Extended Data Fig. 1 |. Mesenchymal *Ptgs2* expression in the microenvironment of crypt stem cells.

a, Transmission electron microscopy photograph of the base of a mouse ileum crypt. P, Paneth cell; S, columnar basal stem cell; F, fibroblast. Scale bar, 5 μm. Indicative of independent observations in two experiments. **b**, Immunostaining for Lgr5–eGFP and Vimentin in the ileum of an *Lgr5-eGFP-IRES-creERT2* mouse. Scale bar, 20 μm. Indicative of independent observations in one experiment. **c**, *PTGS2* relative gene expression (RE) in

intestinal epithelial cells (IECs) and stromal cells isolated from healthy human colonic tissues (n = 6 individuals). Statistical comparison performed with two-tailed Wilcoxon matched-pairs signed-rank test. **d**, *Ptgs2* gene expression in IECs and stromal cells isolated from the ileum and the colon of wild-type mice (n = 4). Statistical significance was determined by two-tailed paired t-test. **e**, Biological replicates of the Drop-seq experiment shown in Fig. 1a visualized on the respective t-SNE plot depicting n = 3,179 mesenchymal cells. Mesenchymal cells were independently isolated from two groups of wild-type mice (biological replicates 1 and 2). From each of these isolations up to three independent Drop-seq samples were collected (A to C) for a total of five samples. **f**, All *Ptgs2*-expressing single cells (n = 1,136) detected in the experiment shown in Fig. 1a, **c** were analysed separately and re-clustered. Cluster annotations are visualized on a t-SNE plot. Violin plots display the entire distribution of gene expression levels per single cell in each cluster for key mesenchymal marker genes. F, fibroblasts. **g**, Schematic representation of the arachidonic acid metabolism pathway. For each mesenchymal cluster shown in Fig. 1a, violin plots display the entire distribution of gene expression levels per single cell for six genes involved in the metabolism of arachidonic acid to prostanoids. Data from n = 3,179 single mesenchymal cells are shown. **h**, Analysis of single-cell RNA-seq data (GSE11434) from the healthy human colonic mesenchyme[3]. Clustering results for n = 4,348 cells and cluster annotations are visualized on a t-SNE plot. The annotations of stromal populations are matched with the ones reported by Kinchen et al.[3] on the basis of the respective markers. Expression levels of *PTGS2* per single cell are visualized on a t-SNE plot. The entire range of gene expression levels per single cell for *PTGS1*, *PTGS2* and key mesenchymal marker genes is displayed in violin plots. Data are mean ± s.e.m.; ns, non-significant; $*P < 0.05$; $**P < 0.01$.

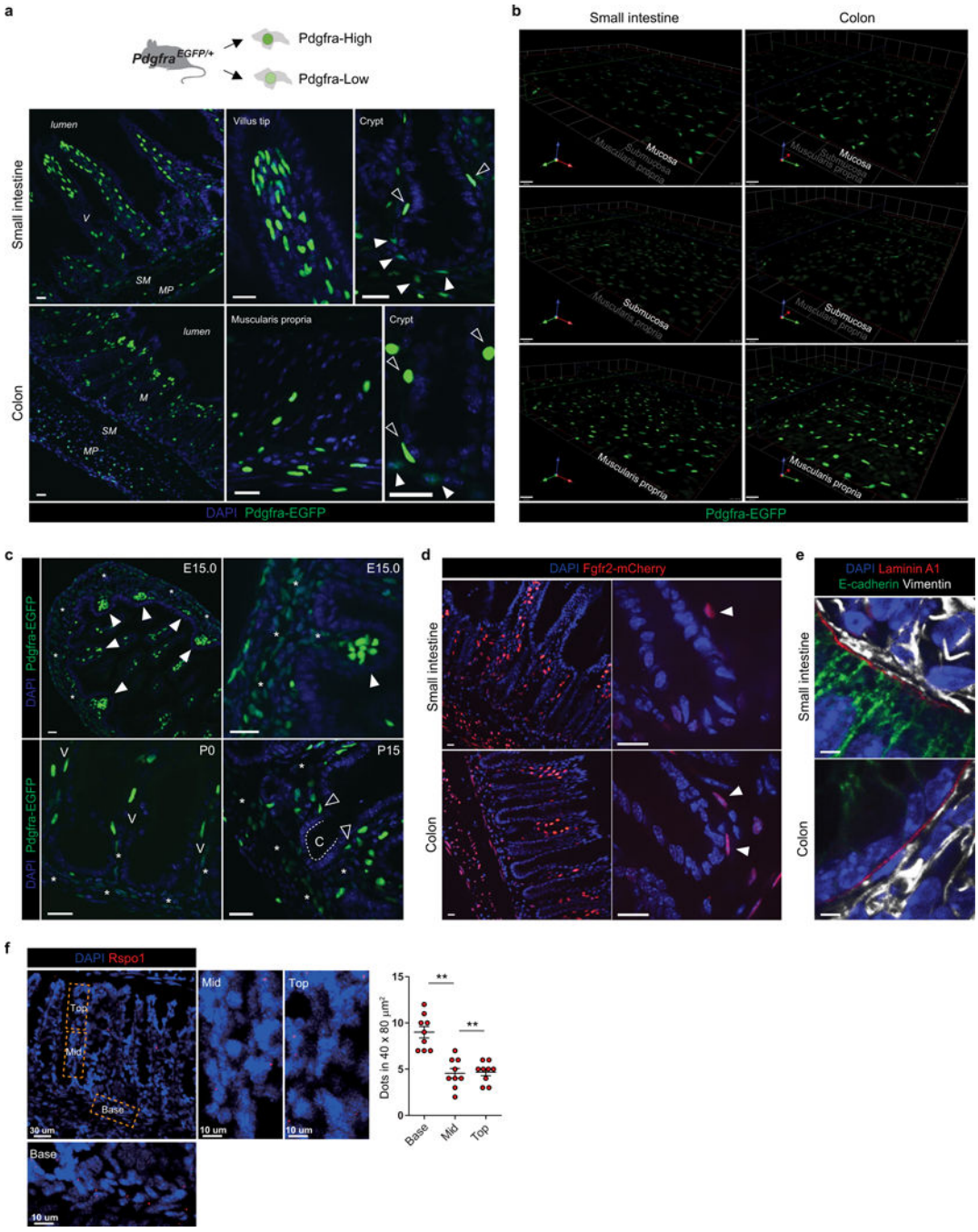

Extended Data Fig. 2 |. Location of major fibroblast populations in the mouse intestine.

a, Detection of *Pdgfra*-expressing mesenchymal cells in the intestine of adult *Pdgfra-H2B-eGPF*-knockin mice[4]. Two distinct populations of Pdgfra^{high} and Pdgfra^{low} mesenchymal cells were detected in fixed tissue sections by direct eGFP fluorescence (green) and confocal microscopy. Nuclei are stained with DAPI (blue). Pdgfra^{high} cells are located under the epithelium along the crypt–villus axis and in the muscularis propria. They form clusters at the tips of villi and the apical part of the colonic mucosa. Pdgfra^{low} cells are located in the inner part of the villi, the pericryptal area and the submucosa. Filled arrows indicate

pericryptal Pdgfra^{low} cells. Open arrows indicate subepithelial Pdgfra^{high} cells. M, mucosa; V, villus; SM, submucosa; MP, muscularis propria. Scale bars, 20 μm. Data are representative of six independent experiments. **b**, Detection of Pdgfra^{high} and Pdgfra^{low} fibroblasts in the fresh, intact intestine of adult *Pdgfra-H2B-eGPF*-knockin mice[4] by two-photon microscopy. The cells were detected by direct eGFP fluorescence (green). Pdgfra^{high} cells are predominant in the muscularis propria, whereas Pdgfra^{low} cells are predominant in the submucosa. Both populations are present in the mucosa. Data are representative of independent observations from one experiment. Scale bars, 100 μm. **c**, Detection of Pdgfra^{high} and Pdgfra^{low} fibroblasts in the intestine of *Pdgfra-H2B-eGPF*-knockin embryos on embryonic day 15 (E15.0) and in early postnatal development. E15.0: clusters of Pdgfra^{high} cells in early villi are indicated by white arrows. Pdgfra^{low} mesenchymal cells occupy the rest of the mesenchyme (asterisks). P0: Pdgfra^{high} cells are observed in the villi (V) and Pdgfra^{low} cells are observed both in the villi and in the rest of the mesenchyme (asterisks). P15: Pdgfra^{low} cells surround an early crypt (C) and Pdgfra^{high} cells are located at the edges of the crypt (open white arrows). Pdgfra^{low} cells occupy the inner mesenchyme (asterisks). Data are representative of independent observations from one experiment per developmental stage. Scale bars, 20 μm. **d**, The location of *Fgfr2*-expressing mesenchymal cells was determined in the intestine of an *Fgfr2-T2A-H2B-mCherry*-knockin mouse[5], by detecting direct mCherry fluorescence (red) in the nucleus (blue, DAPI). The arrows indicate pericryptal Fgfr2^{+} fibroblasts. Data are representative of independent observations from one experiment. Scale bars, 20 μm. **e**, Immunostaining for laminin A1 (encoded by *Lama1*), the epithelial marker E-cadherin and the mesenchymal marker vimentin in the normal mouse intestines shows that laminin A1 is detected specifically at the mesenchymal–epithelial interface. Data are representative of two independent experiments. Scale bars, 5 μm. **f**, In-situ hybridization analysis showing the location of *Rspo1*-expressing cells in the normal mouse colon. The position of *Rspo1*-expressing cells along the crypt axis was quantified in 40 × 80 μm^2 sub-epithelial areas at the base, middle and top sections of $n = 9$ crypts. Unpaired two-tailed Student's *t*-test. Mean ± s.e.m. $^{**}P < 0.01$.

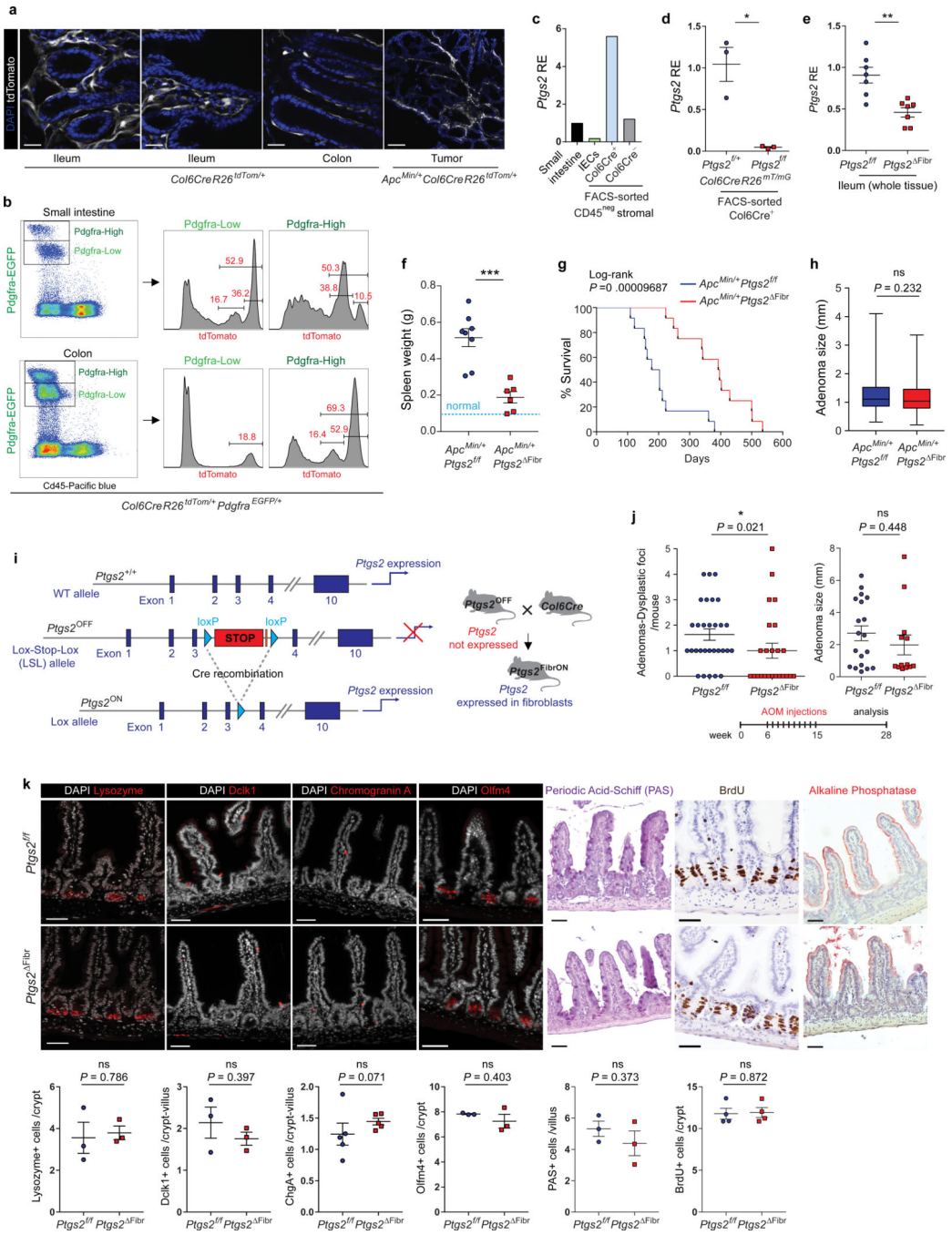

Extended Data Fig. 3 |. Mice with fibroblast-specific ablation or fibroblast-restricted expression of Ptgs2.

a, Immunofluorescence of ileum and colon sections from *Col6-Cre-Rosa26*$^{tdTomato/+}$ mice (scale bar, 20 μm) and of a small intestinal tumour section from an *Apc*$^{Min/+}$*-Col6-Cre-Rosa26*$^{tdTomato/+}$ mouse (scale bar, 150 μm). Data are representative of two experiments. **b**, Efficiency of *Col6-Cre*-mediated recombination of a lox-stop-lox tdTomato reporter in Pdgfra^{high} and Pdgfra^{low} Cd45^{-} cells determined by flow cytometry in intestinal mesenchymal and lamina propria cells isolated from the small intestine and the colon of

Col6-Cre-Rosa26$^{tdTomato/+}$*Pdgfra*$^{eGFP/+}$ mice in one experiment. **c**, *Ptgs2* gene expression in whole tissue, isolated IECs, FACS-sorted *Col6Cre*$^{+}$ fibroblasts (CD45^{-}tdTomato^{+}) and *Col6Cre*$^{-}$ mesenchymal cells (CD45^{-}tdTomato^{-}) from the small intestine of *Col6-Cre-Rosa26*$^{tdTomato/+}$ mice (n = 3, pooled). Representative of two experiments. **d**, Efficiency of *Col6-Cre*-mediated *Ptgs2* gene ablation in Col6-Cre^{+} mesenchymal cells determined by RT–qPCR analysis of *Ptgs2* expression in FACS-sorted *Col6-Cre*$^{+}$ fibroblasts (eGFP^{+}) from the small intestine of *Col6-Cre-Rosa26*$^{mT/mG}$*Ptgs2*$^{f/+}$ (n = 3) and *Col6-Cre-Rosa26*$^{mT/mG}$*Ptgs2*$^{f/f}$ (n = 3) mice. Unpaired two-tailed Welch's t-test. **e**, Expression of the *Ptgs2* gene in whole tissue ileum of littermate *Ptgs2*$^{f/f}$ and *Ptgs2*$^{\Delta Fibr}$ mice (n = 7 each). Two-tailed t-test. **f**, Spleen weight of 5.5-month-old *Apc*$^{Min/+}$*Ptgs2*$^{f/f}$ (n = 8) and *Apc*$^{Min/+}$*Ptgs2*$^{\Delta Fibr}$ (n = 6) mice. Average spleen weight of (n = 6) normal littermates (*Ptgs2*$^{f/f}$) is displayed for comparison. Two-tailed t-test. **g**, Survival analysis of *Apc*$^{Min/+}$*Ptgs2*$^{f/f}$ (n = 12) and *Apc*$^{Min/+}$*Ptgs2*$^{\Delta Fibr}$ (n = 12) mice. A two-tailed P = 0.00009687 was calculated by log-rank test. **h**, Size of 274 adenomas from 5.5-month-old *Apc*$^{Min/+}$*Ptgs2*$^{f/f}$ (n = 16) and *Apc*$^{Min/+}$*Ptgs2*$^{\Delta Fibr}$ (n = 18) mice. The whiskers extend from minimum to maximum and the box extends from the 25th to 75th percentiles with the median indicated. Two-tailed Mann–Whitney test. **i**, Generation of knockin mice bearing a lox-stop-lox cassette insertion in intron-3 of the *Ptgs2* gene which prevents its expression (*Ptgs2*^{OFF}). *Col6-Cre*-mediated excision of the lox-stop-lox cassette reactivates *Ptgs2* expression specifically in fibroblasts (*Ptgs2*^{FibrON}). The orange box depicts an frt site remaining from the flp-mediated removal of an frt-flanked PGK-neomycin selection cassette (see Methods). **j**, *Ptgs2*$^{f/f}$ (n = 30) and *Ptgs2*$^{\Delta Fibr}$ (n = 24) mice were subjected to 10 weekly intraperitoneal injections with 10 mg kg^{-1} azoxymethane as displayed. Quantification of the number of dysplastic foci and microadenomas per mouse and quantification of tumour size is shown. Statistical significance was tested by two-tailed Mann–Whitney test. **k**, Quantification of intestinal epithelial populations in the ileum of littermate *Ptgs2*$^{f/f}$ and *Ptgs2*$^{\Delta Fibr}$ mice (n = 3–5 per genotype). Immunostaining was performed for markers of Paneth cells (lysozyme), tuft cells (Dclk1), enteroendocrine cells (chromogranin A) and stem cells (Olfm4). Goblet cells were identified by periodic acid Schiff (PAS) staining and enterocytes were identified by detecting alkaline phosphatase enzymatic activity. Incorporation and immunohistochemical detection of BrdU was used to determine the numbers of cycling cells. Data for each mouse represent mean number of positive cells per crypt or crypt–villus unit as indicated. N = 400–822 crypts and villi were evaluated per staining. Statistical comparisons were performed with two-tailed unpaired t-test except for Olfm4^{+} cells for which unpaired t-test with Welch's correction was applied. Scale bars, 50 μm. All data represent mean ± s.e.m. unless otherwise indicated. ns, non-significant; *P < 0.05, **P < 0.01, ***P < 0.001.

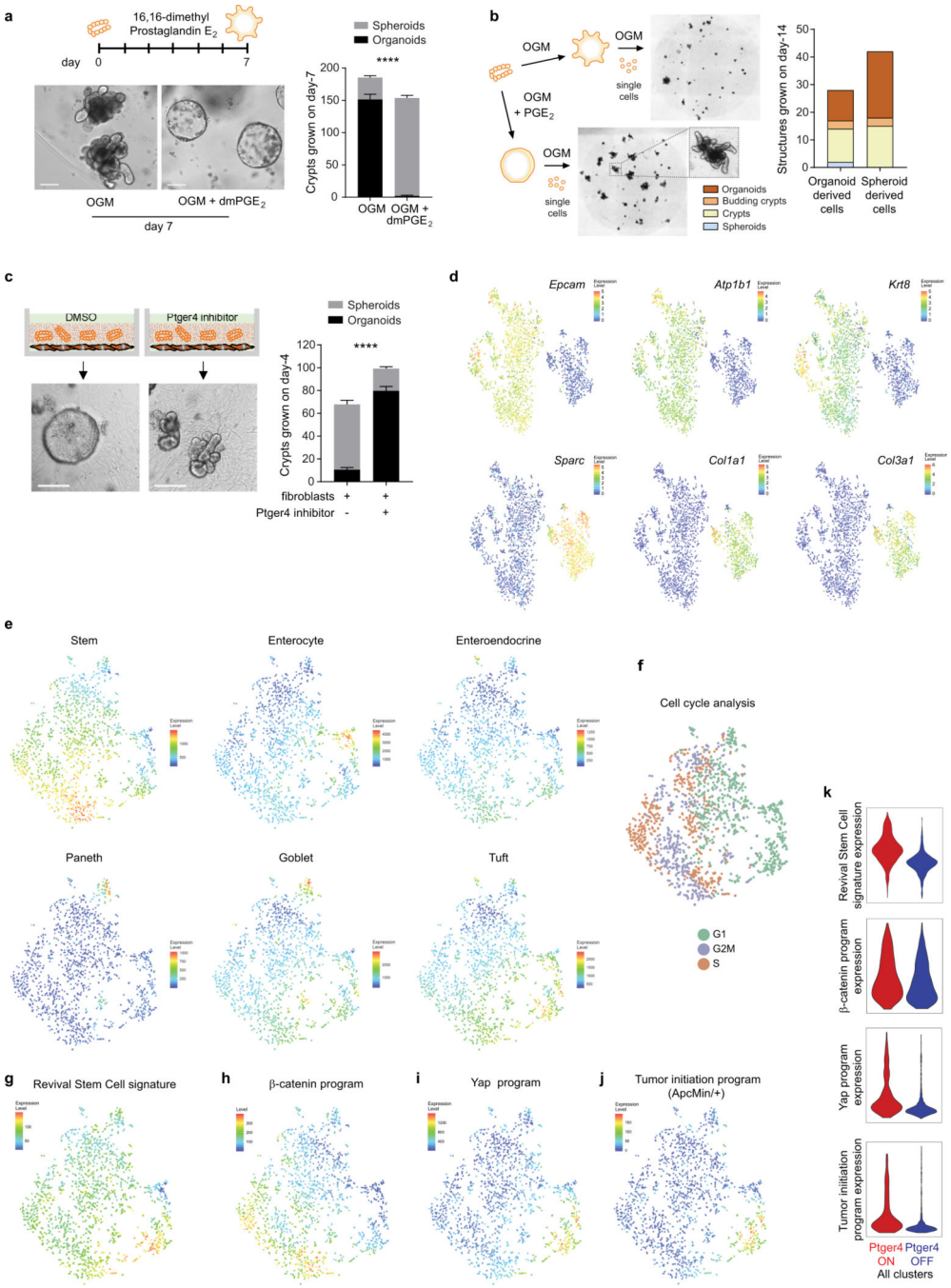

Extended Data Fig. 4 |. PGE_2-driven spheroids contain more functional stem cells.

a, Crypts isolated from the small intestine of wild-type mice were grown into organoids by 3D culture with OGM or OGM that was supplemented daily with 0.1 μM 16,16-dimethyl PGE_2 ($dmPGE_2$). Indicative images and quantification of the absolute numbers of organoids and spheroids grown per 3D structure are shown. $n = 6$ 3D cultures were evaluated per condition. Scale bar, 100 μm. **b**, Assessment of stem cell activity in organoids or PGE_2-driven spheroids grown as in **a** by dissociation into single cells and 3D culture in OGM. Growth of crypts and organoids from the same initial number of cells was quantified on day

14. The results are indicative of five independent experiments starting from independent crypt isolations. **c**, Normal crypts were grown into organoids with OGM in a 3D co-culture with primary mouse intestinal fibroblasts with or without 10 μM ONO-AE3–208 (Ptger4/EP4 inhibitor). Indicative images and quantification of the absolute numbers of organoids and spheroids grown per 3D structure are shown. $n = 6$ 3D co-cultures were evaluated per condition. Scale bar, 200 μm. **d**, Separation of $n = 2{,}192$ fibroblasts and epithelial cells in single-cell RNA-seq data from fibroblast–crypt organotypic cultures on the basis of the expression of key marker genes. Expression of intestinal epithelial marker genes (*Epcam*, *Atp1b1* and *Krt8*) and fibroblast marker genes (*Sparc*, *Col1a1* and *Col3a1*) in single cells from Ptger4-ON and Ptger4–OFF fibroblast–crypt co-cultures is shown projected onto *t*-SNE plots. **e–j**, Single-cell data from Ptger4-ON and Ptger4–OFF fibroblast–crypt co-cultures as shown in Fig. 3d, visualized on the respective *t*-SNE plot depicting $n = 1{,}585$ epithelial cells. **e**, Expression of epithelial population-specific signatures (metagenes) per single epithelial cell. Population signatures were calculated on the basis of single-cell profiling of the mouse intestinal epithelium[15]. **f**, Cell cycle analysis of single epithelial cells projected onto the *t*-SNE plot. **g–j**, Expression levels of metagenes for the signatures or transcriptional programs of RSC[16] (**g**), β-catenin (**h**), Yap (**i**) and early (non-tumour) $Apc^{min/+}$ (**j**) tumorigenesis per single epithelial cell projected onto *t*-SNE plots. **k**, Data from $n = 1{,}585$ single epithelial cells, visualized in violin plots for each co-culture condition (Ptger4-ON or Ptger4-OFF). The entire range of metagene expression levels per single epithelial cell for the signatures or transcriptional programs of RSCs, β-catenin, Yap and early $Apc^{min/+}$ tumorigenesis is displayed. In **a**, **c**, two-way ANOVA. Data are mean ± s.e.m. **** $P < 0.0001$.

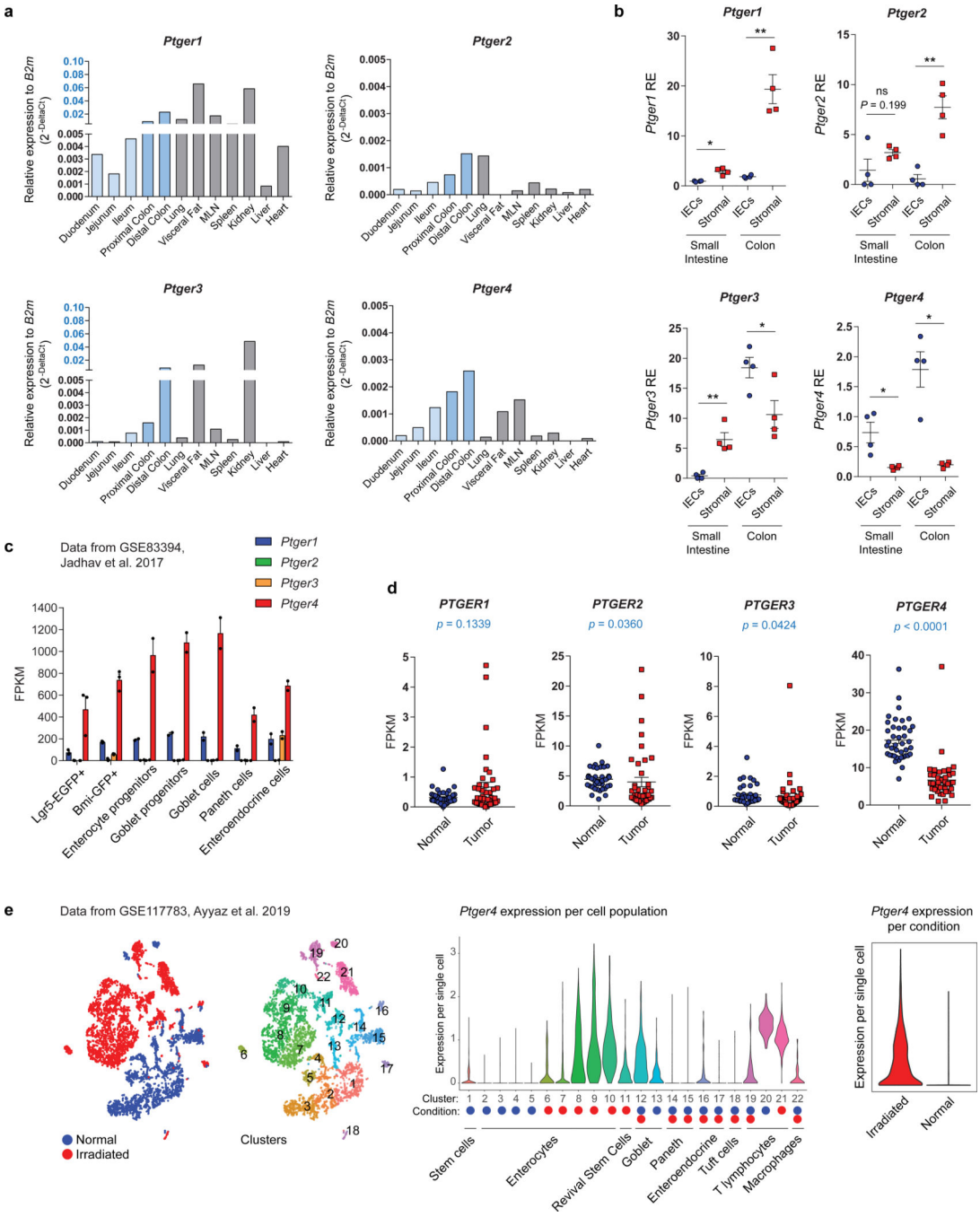

Extended Data Fig. 5 |. Expression of PGE_2 receptors in mouse and human tissues.

a, RT–qPCR analysis for *Ptger1*, *Ptger2*, *Ptger3* and *Ptger4* genes across 12 mouse tissues. Expression relative to *B2m* is displayed as $2^{-\Delta Ct}$. Data represent one experiment. **b**, RT–qPCR analysis for *Ptger1*, *Ptger2*, *Ptger3* and *Ptger4* genes in isolated IECs and matched stromal fractions from the small intestine (ileum) and the colon of wild-type mice ($n = 4$). Statistical comparisons were performed by two-tailed paired *t*-test. **c**, Expression levels of *Ptger1*, *Ptger2*, *Ptger3* and *Ptger4* genes determined by RNA-seq in FACS-sorted intestinal epithelial cell populations in 2 or 3 biological replicates and displayed as FPKM (fragments

per kilobase of transcript per million mapped reads). Data retrieved from the GSE83394 GEO dataset. **d**, Expression levels of the human *PTGER1*, *PTGER2*, *PTGER3* and *PTGER4* genes in matched normal colon and tumour tissues from colorectal cancer patients ($n = 41$), determined by RNA-seq and displayed as FPKM. Data retrieved from The Cancer Genome Atlas for colon adenocarcinoma (TCGA–COAD dataset). Statistical comparisons were performed by two-tailed Wilcoxon matched-pairs signed-rank test. **e**, Analysis of single-cell RNA-seq data[16] (GSE117783) from crypts isolated from the small intestine of normal mice (blue) and mice treated with 12 Gy irradiation (red). $n = 6{,}644$ single cells are visualized on *t*-SNE plots based on the experimental condition (normal, $n = 2{,}882$; irradiated, $n = 3{,}762$) and the clustering results. Violin plots represent the entire distribution of *Ptger4* expression levels per single cell in each cluster and in each condition. The annotations of epithelial populations are matched with the ones reported by Ayyaz et al.[16] on the basis of the respective markers. **b–d**, Mean ± s.e.m.; ns, non-significant; $*P < 0.05$; $**P < 0.01$.

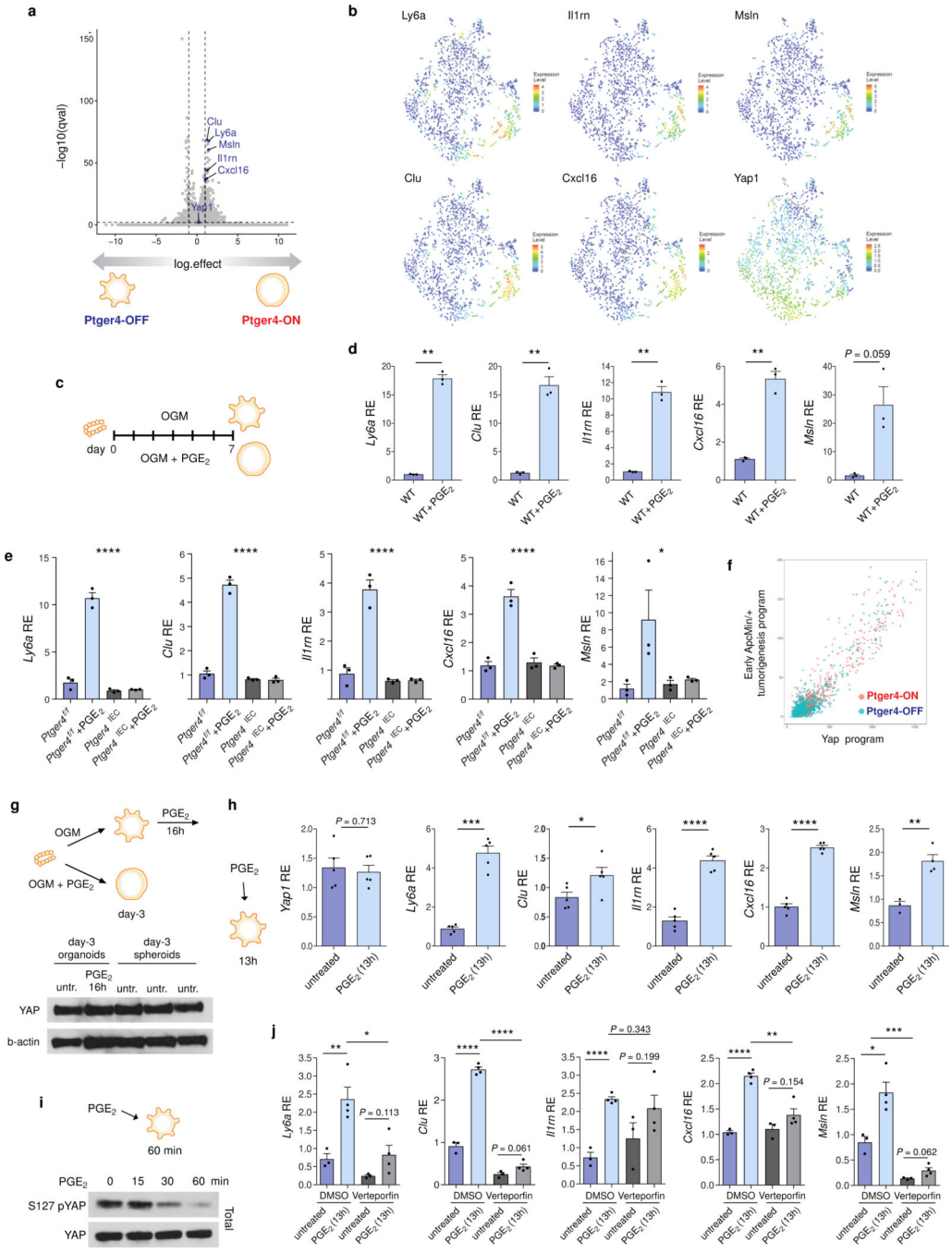

Extended Data Fig. 6 |. PGE_2–Ptger4 drive the induction of Yap target genes in intestinal organoids.

a, Volcano plot displaying the results of differential gene-expression analysis performed in single epithelial cells from Ptger4-ON and Ptger4–OFF fibroblast–crypt co-cultures (n = 1,585). *Yap1* and Yap target genes[18] are indicated. Moderated t-test with false-discovery rate (Benjamini–Hochberg) correction. **b**, Expression levels of the genes indicated in single epithelial cells from Ptger4-ON and Ptger4–OFF fibroblast–crypt co-cultures (n = 1,585), projected onto t-SNE plots. **c**, Experimental setup for data shown in **d**, **e**. Crypts were grown

into organoids or spheroids by 3D culture in OGM or OGM that was supplemented daily with 0.1 μM $dmPGE_2$ for 7 days. Gene expression levels were measured by RT–qPCR on day 7. **d**, Relative expression of Yap target genes (*Ly6a*, *Clu*, *Il1rn*, *Msln* and *Cxcl16*) in day 7 organoids and PGE_2-driven spheroids developed from wild-type crypts. $N = 3$ 3D cultures per condition. Two-tailed Welch's *t*-test. **e**, Relative expression of Yap target genes in day 7 organoids and PGE_2-driven spheroids developed from crypts isolated from $Ptger4^{f/f}$ and $Ptger4^{\Delta IEC}$ mice. $n = 3$ 3D cultures per genotype and condition. One-way ANOVA. **f**, Correlation between the expression levels of metagenes of a Yap transcriptional program and an early (non-tumour) $Apc^{min/+}$ tumorigenesis transcriptional program in single epithelial cells ($n = 1{,}585$) from the Ptger4-ON and Ptger4–OFF fibroblast–crypt co-cultures of Fig. 3. **g**, Small intestinal crypts were grown into organoids or spheroids with OGM or OGM that was supplemented daily with 0.1 μM $dmPGE_2$. Western blot analysis for Yap1 and β-actin was performed in total lysates from untreated organoids, organoids treated with 0.1 μM $dmPGE_2$ for 16 h and untreated spheroids. Data from one organoid and three independent spheroid cultures. **h**, Relative expression of the *Yap1* gene and Yap target genes in wild-type organoid cultures treated with 0.1 μM $dmPGE_2$ for 13 h, as determined by RT–qPCR. $n = 3$–5 cultures per condition. Statistical comparisons were performed with unpaired two-tailed *t*-test. For *Ly6a*, Welch's correction was applied. **i**, Western blot analysis for Ser127 pYap and total Yap performed in total lysates from wild-type organoids stimulated with 0.1 μM $dmPGE_2$ for the indicated time-points. Indicative of five independent experiments. **j**, Relative expression of Yap target genes in wild-type organoids treated with 1 μM verteporfin and 0.1 μM $dmPGE_2$ for 13 h. $n = 3$–4 cultures per condition. Statistical comparisons were performed with unpaired two-tailed *t*-test, two-tailed Welch's *t*-test or Mann–Whitney test on the basis of the criteria described in Methods. All data are mean ± s.e.m. $*P < 0.05$, $**P < 0.01$, $***P < 0.001$, $****P < 0.0001$.

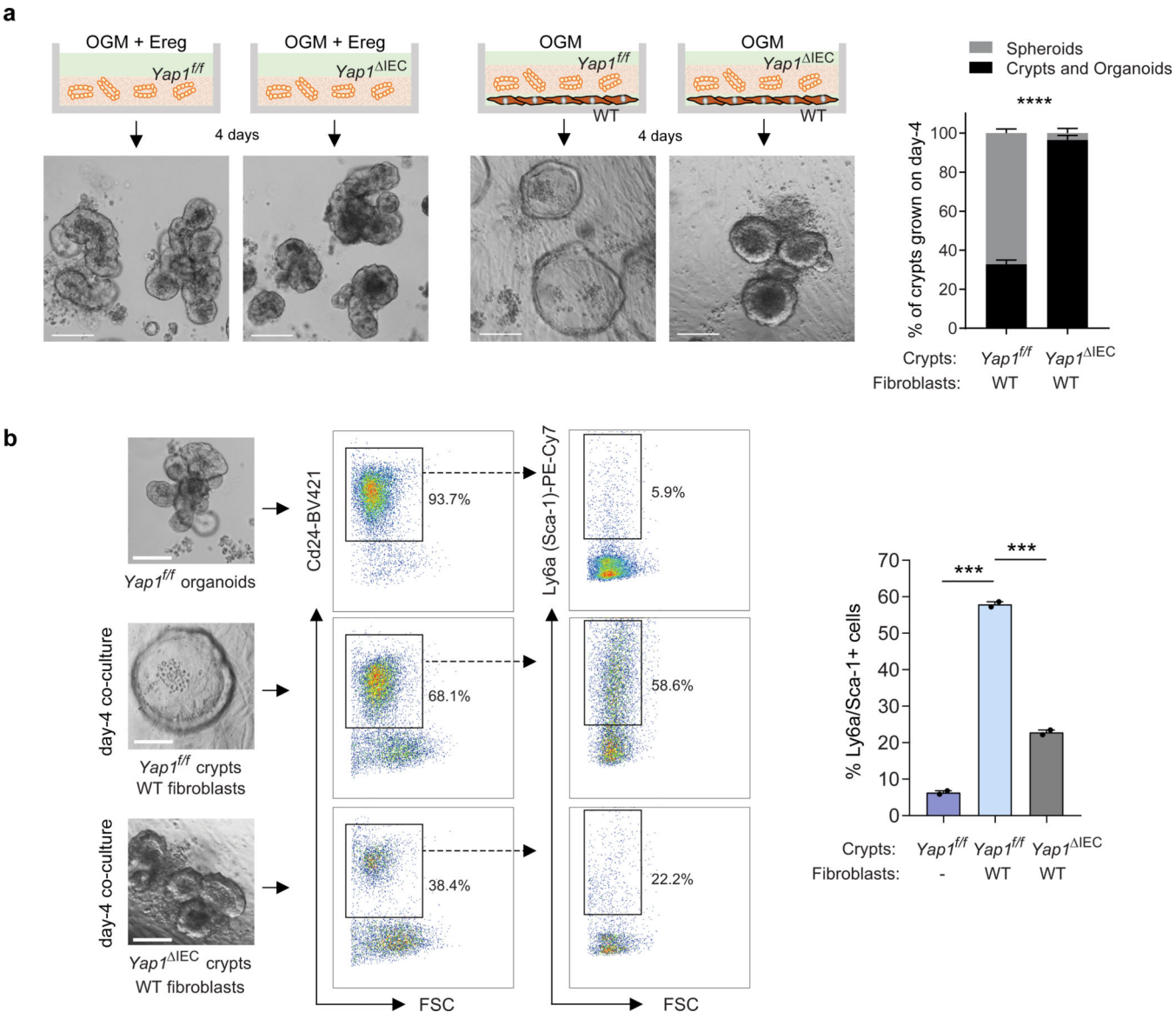

Extended Data Fig. 7 |. Genetic ablation of Yap prevents spheroid formation and Sca-1$^+$ stem cell expansion in fibroblast–crypt organotypic co-cultures.

a, Crypts isolated from the small intestines of *Yap1$^{f/f}$* and *Yap1$^{\Delta IEC}$* mice were grown into organoids by 3D culture with OGM supplemented with 0.5 mg ml^{-1} recombinant mouse epiregulin (Ereg) as previously described[18], or in a co-culture with wild-type primary mouse intestinal fibroblasts with OGM without Ereg supplementation. Indicative images and quantification of the percentages of crypts, organoids and spheroids grown per 3D structure are shown. $n = 2$ cultures per condition. Data are representative of two independent experiments. Scale bars, 100 μm. Two-way ANOVA. Data represent mean ± s.e.m. ****$P <$ 0.0001. **b**, Intestinal crypts isolated from the small intestines of *Yap1$^{f/f}$* and *Yap1$^{\Delta IEC}$* mice were co-cultured with wild-type primary mouse intestinal fibroblasts. On day 4, these co-cultures and control *Yap1$^{f/f}$* organoid cultures were processed into single-cell suspensions and analysed by flow cytometry for Sca-1 expression in Cd24$^+$ epithelial cells. $n = 2$ cultures

per condition. Scale bars, 100 μm. FSC, forward scatter. Unpaired two-tailed *t*-test. Mean ± s.e.m. *** $P < 0.001$.

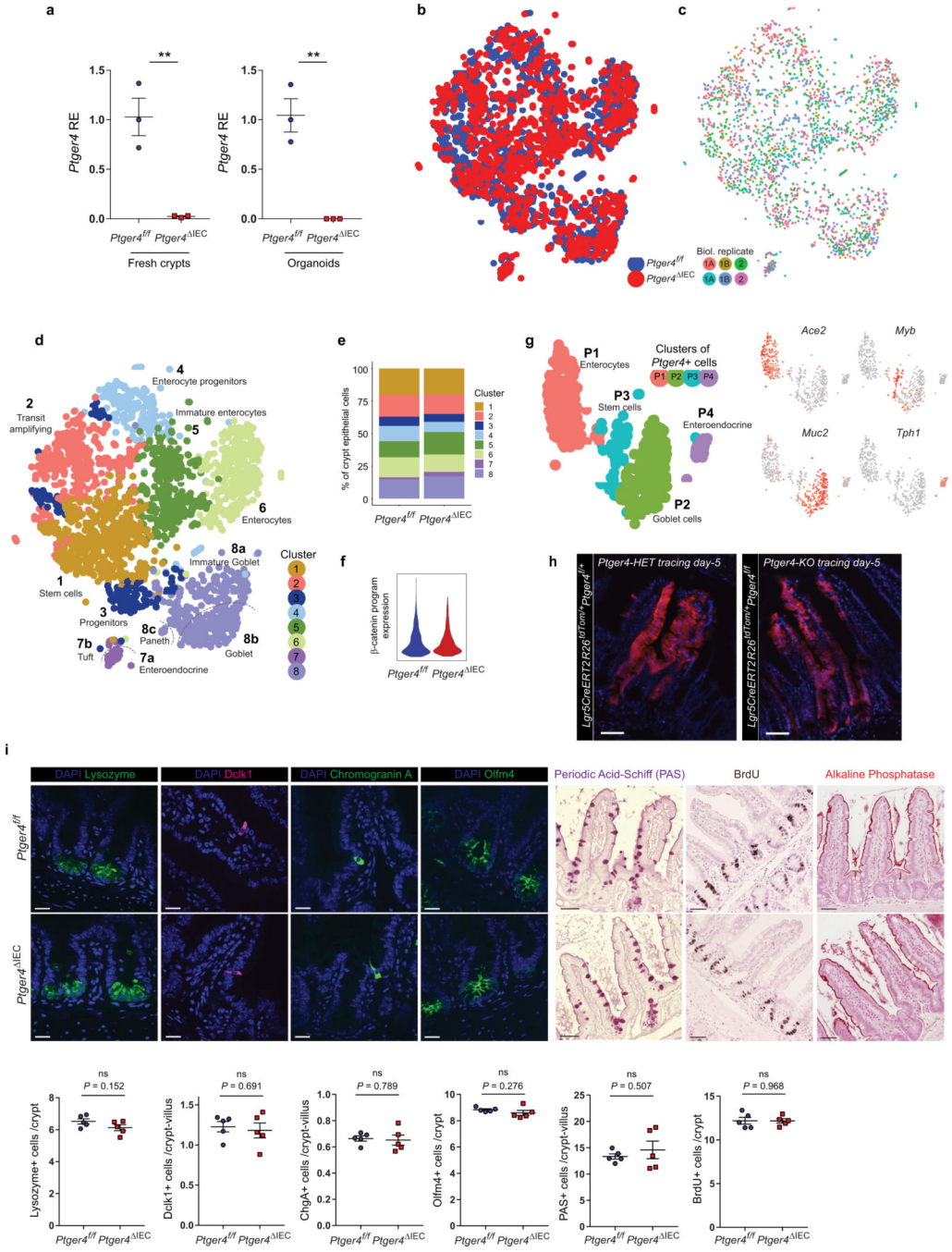

Extended Data Fig. 8 |. Ptger4 ablation does not affect epithelial lineage differentiation and stem cell function.

a, *Ptger4* gene expression in crypts isolated from the ileum of littermate *Ptger4*$^{f/f}$ and *Ptger4*$^{\Delta IEC}$ mice ($n = 3$ mice per genotype) and in organoids grown from these crypts ($n = 3$ cultures per genotype) determined by RT–qPCR analysis. Two-tailed unpaired *t*-test. **b**, Single-cell RNA-seq (Drop-seq) was performed in crypt epithelial cells isolated from

littermate *Ptger4*$^{f/f}$ and *Ptger4*$^{\Delta IEC}$ mice. Data for 2,439 single epithelial cells are shown in a *t*-SNE plot. **c**, Biological replicates visualized on a *t*-SNE plot. Crypt epithelial cells were independently isolated from two groups of mice per genotype (biological replicates 1 and 2). From the first biological replicate, two independent Drop-seq samples were collected (A and B) for a total number of three samples per genotype. **d**, Clustering and cluster assignments of 2,439 single epithelial cells displayed on a *t*-SNE plot. **e**, Proportion of each epithelial cluster among total crypt epithelial cells in *Ptger4*$^{f/f}$ and *Ptger4*$^{\Delta IEC}$ mice. **f**, Violin plots showing the entire range of expression levels for a metagene of the β-catenin transcriptional program in $n = 2,439$ single epithelial cells from *Ptger4*$^{f/f}$ and *Ptger4*$^{\Delta IEC}$ mice. **g**, Analysis of all *Ptger4*-expressing single cells detected ($n = 478$). Re-clustering results of *Ptger4*-expressing single cells with cluster annotations are visualized on a *t*-SNE plot. The expression levels of key marker genes for these clusters are visualized on *t*-SNE plots. **h**, Lineage tracing of *Ptger4* heterozygous (*Ptger4*-HET) and *Ptger4*-knockout (*Ptger4*-KO) Lgr5^{+} stem cells. The small intestines of *Lgr5-CreERT2-Rosa26*$^{tdTomato/+}$*Ptger4*$^{f/+}$ (*Ptger4*-HET) and *Lgr5-CreERT2-Rosa26*$^{tdTomato/+}$*Ptger4*$^{f/f}$ (*Ptger4*-KO) mice were examined for direct tdTomato fluorescence 5 days after a single injection of 2 mg tamoxifen per mouse. The results shown are representative of independent observations from one experiment. Scale bars, 70 μm. **i**, Quantification of intestinal epithelial populations in the ileum of littermate *Ptger4*$^{f/f}$ ($n = 5$) and *Ptger4*$^{\Delta IEC}$ ($n = 5$) mice. Immunostaining was performed for markers of Paneth cells (lysozyme), tuft cells (Dclk1), enteroendocrine cells (chromogranin A) and stem cells (Olfm4). Scale bars, 20 μm. Goblet cells were identified by PAS staining and enterocytes were detected by alkaline phosphatase enzymatic activity. Scale bars, 50 μm. Incorporation and immunohistochemical detection of BrdU was used to determine the numbers of cycling cells. Scale bars, 50 μm. Data for each mouse represent mean number of positive cells per crypt or crypt–villus unit as indicated. $n = 217–565$ crypts and villi were evaluated per staining. Statistical comparisons were performed with two-tailed unpaired *t*-test except for PAS^{+} cells, for which unpaired Welch's *t*-test was applied. Mean ± s.e.m.; ns, non-significant; $^{**}P < 0.01$.

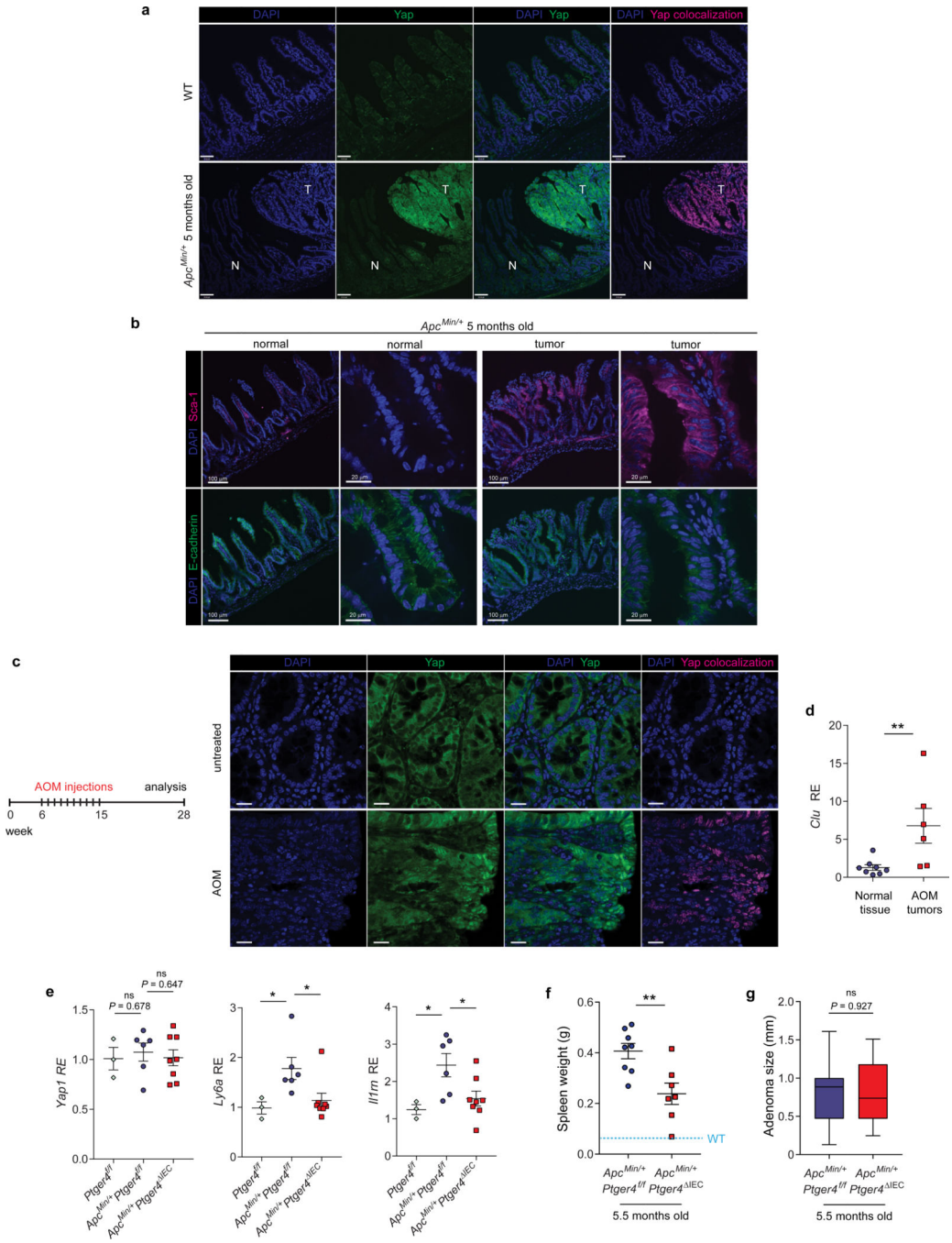

Extended Data Fig. 9 |. Nuclear localization of Yap and activation of Yap target genes in *Apc*$^{Min/+}$ and azoxymethane-induced tumorigenesis.

a, Immunostaining for Yap in the small intestine of five-month-old *Apc*$^{Min/+}$ and wild-type littermate control mice. Nuclear localization of Yap is displayed on the basis of colocalization with DAPI. Normal (N) and Tumour (T) areas of the *Apc*$^{Min/+}$ intestine are indicated. Scale bars, 70 μm. Data are indicative of at least ten different tumour areas. **b**, Immunostaining for Sca-1 and the epithelial marker E-cadherin in normal and tumour areas of the small intestine of five-month-old *Apc*$^{Min/+}$ mice. Indicative of two independent

experiments. **c**, Immunostaining for Yap in the colon of wild-type mice subjected to 10 weekly intraperitoneal injections with 10 mg kg^{-1} azoxymethane as indicated and in untreated controls. Nuclear localization of Yap is displayed on the basis of colocalization with DAPI. Scale bars, 20 μm. Data indicative of three mice analysed. **d**, Relative expression of the Yap target gene *Clu* in normal and tumour areas of the colon of wild-type mice ($n = 8$) subjected to 10 weekly intraperitoneal injections with 10 mg kg^{-1} azoxymethane as shown in **c**. Two-tailed Mann–Whitney test. **e**, Relative expression of *Yap1* and Yap target genes in the small intestine of 5-week-old $Ptger4^{f/f}$ ($n = 3$), $Apc^{Min/+}Ptger4^{f/f}$ ($n = 6$) and $Apc^{Min/+}Ptger4^{\Delta IEC}$ ($n = 8$) mice. Statistical comparisons were performed with two-tailed *t*-test for *Yap1* and *Il1rn* and with two-tailed Mann–Whitney test for *Ly6a*. **f**, Spleen weight of 5.5-month-old $Apc^{Min/+}Ptger4^{f/f}$ ($n = 8$) and $Apc^{Min/+}Ptger4^{\Delta IEC}$ ($n = 7$) mice. Average spleen weight of ($n = 2$) normal littermates ($Ptger4^{f/f}$) is displayed for comparison. Two-tailed *t*-test. **g**, Size of 72 adenomas from 5.5-month-old $Apc^{Min/+}Ptger4^{f/f}$ ($n = 6$) and $Apc^{Min/+}Ptger4^{\Delta IEC}$ ($n = 4$) mice. The whiskers extend from minimum to maximum and the box extends from the 25th to 75th percentiles with the median indicated. Two-tailed Mann–Whitney test. Mean ± s.e.m.; ns, non-significant; $*P < 0.05$; $**P < 0.01$.

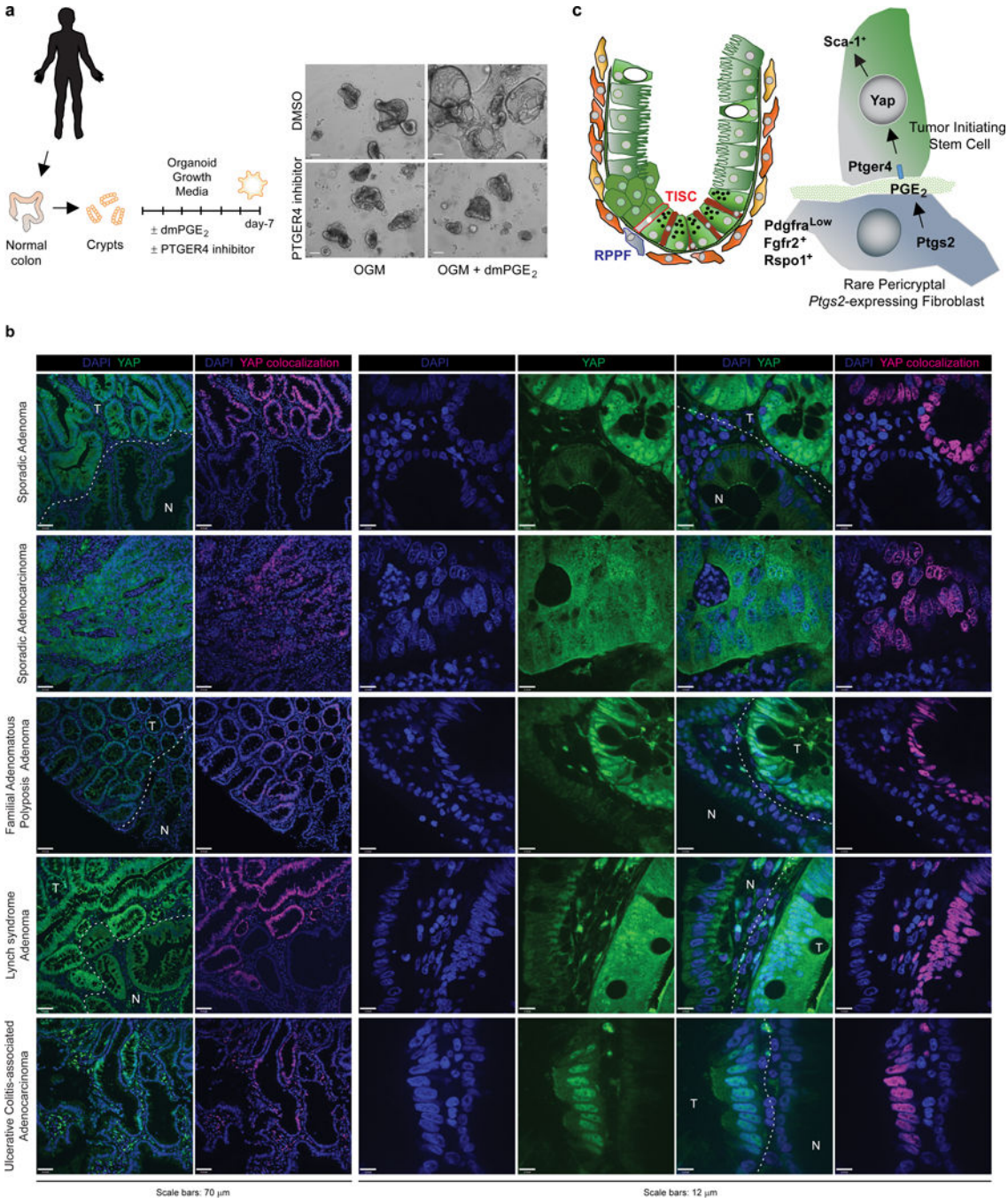

Extended Data Fig. 10 |. PGE $_2$–PTGER4 controls stem cell function in human colonic crypts and YAP displays a nuclear localization in human colorectal tumours.

a, Human colonic crypts were grown into organoids by 3D culture with OGM or OGM supplemented daily with 0.1 μM $dmPGE_2$, with or without 10 μM ONO-AE3–208 (PTGER4–EP4 inhibitor). Images indicative of three independent experiments with crypts isolated from three patients are shown. Scale bar, 100 μm. **b**, Immunostaining for YAP in sections of human colorectal adenomas or adenocarcinomas and neighbouring normal tissue areas. Nuclear localization of Yap is displayed on the basis of colocalization with DAPI.

Clearly defined normal (N) and tumour (T) areas are indicated wherever applicable. Images shown are representative of specimens obtained and analysed from $n = 16$ patients with the types of colorectal tumours indicated. Patient characteristics and the type of colorectal tumour per individual are described in the Supplementary Table 3. **c**, Schematic representation of the mechanism proposed in the present study. TISC, tumour-initiating stem cell.

Supplementary Material

Refer to Web version on PubMed Central for supplementary material.

Acknowledgments

We thank C. Lieber, J. Alderman and E. Hughes-Picard for administrative assistance; the Yale Pathology Tissue Service–Tissue Procurement and Distribution Facility for providing human tissue samples; D. Gonzalez for assistance in two-photon imaging; M. Graham for assistance in electron microscopy; M. Samiotaki and T. Wu for assistance in mass spectrometry; and Flavell laboratory members R. Jackson and W. Bailis for discussions. M.R. is supported by a Crohn's and Colitis Foundation Career Development Award (510777); M.S., L.-S.F., M.S.K. and M.B. were supported by an Austrian Marshall Plan Foundation Master's Fellowship. This work was supported in part by ERC project MCs-inTEST (340217) (G.K.), the National Natural Science Foundation of China (31930035, 91942311) (B.S.), the Blavatnik Family Foundation and the Howard Hughes Medical Institute (R.A.F.).

References

1. Vermeulen L & Snippert HJ Stem cell dynamics in homeostasis and cancer of the intestine. Nat. Rev. Cancer 14, 468–480 (2014). [PubMed: 24920463]
2. Powell DW, Pinchuk IV, Saada JI, Chen X & Mifflin RC Mesenchymal cells of the intestinal lamina propria. Annu. Rev. Physiol. 73, 213–237 (2011). [PubMed: 21054163]
3. Kinchen J et al. Structural remodeling of the human colonic mesenchyme in inflammatory bowel disease. Cell 175, 372–386 (2018). [PubMed: 30270042]
4. Hamilton TG, Klinghoffer RA, Corrin PD & Soriano P Evolutionary divergence of platelet-derived growth factor alpha receptor signaling mechanisms. Mol. Cell. Biol. 23, 4013–4025 (2003). [PubMed: 12748302]
5. Molotkov A, Mazot P, Brewer JR, Cinalli RM & Soriano P Distinct requirements for FGFR1 and FGFR2 in primitive endoderm development and exit from pluripotency. Dev. Cell. 41, 511–526 (2017). [PubMed: 28552557]
6. Smyth EM, Grosser T, Wang M, Yu Y & FitzGerald GA Prostanoids in health and disease. J. Lipid Res. 50 (Suppl), S423–S428 (2009). [PubMed: 19095631]
7. Wang D & DuBois RN The role of anti-inflammatory drugs in colorectal cancer. Annu. Rev. Med. 64, 131–144 (2013). [PubMed: 23020877]
8. Barker N et al. Crypt stem cells as the cells-of-origin of intestinal cancer. Nature 457, 608–611 (2009). [PubMed: 19092804]
9. Chulada PC et al. Genetic disruption of Ptgs-1, as well as Ptgs-2, reduces intestinal tumorigenesis in Min mice. Cancer Res. 60, 4705–4708 (2000). [PubMed: 10987272]
10. Cherukuri DP et al. Targeted Cox2 gene deletion in intestinal epithelial cells decreases tumorigenesis in female, but not male, ApcMin/+ mice. Mol. Oncol. 8, 169–177 (2014). [PubMed: 24268915]
11. Xia D, Wang D, Kim SH, Katoh H & DuBois RN Prostaglandin E_2 promotes intestinal tumor growth via DNA methylation. Nat. Med. 18, 224–226 (2012). [PubMed: 22270723]
12. Wang D, Fu L, Sun H, Guo L & DuBois RN Prostaglandin E2 promotes colorectal cancer stem cell expansion and metastasis in mice. Gastroenterology 149, 1884–1895 (2015). [PubMed: 26261008]
13. Bygdeman M Pharmacokinetics of prostaglandins. Best Pract. Res. Clin. Obstet. Gynaecol. 17, 707–716 (2003). [PubMed: 12972009]

14. Mustata RC et al. Identification of Lgr5-independent spheroid-generating progenitors of the mouse fetal intestinal epithelium. Cell Rep. 5, 421–432 (2013). [PubMed: 24139799]
15. Haber AL et al. A single-cell survey of the small intestinal epithelium. Nature 551, 333–339 (2017). [PubMed: 29144463]
16. Ayyaz A et al. Single-cell transcriptomes of the regenerating intestine reveal a revival stem cell. Nature 569, 121–125 (2019). [PubMed: 31019301]
17. Miyoshi H et al. Prostaglandin E2 promotes intestinal repair through an adaptive cellular response of the epithelium. EMBO J. 36, 5–24 (2017). [PubMed: 27797821]
18. Gregorieff A, Liu Y, Inanlou MR, Khomchuk Y & Wrana JL Yap-dependent reprogramming of $Lgr5^{+}$ stem cells drives intestinal regeneration and cancer. Nature 526, 715–718 (2015). [PubMed: 26503053]
19. Hong AW, Meng Z & Guan KL The Hippo pathway in intestinal regeneration and disease. Nat. Rev. Gastroenterol. Hepatol. 13, 324–337 (2016). [PubMed: 27147489]
20. Cai J, Maitra A, Anders RA, Taketo MM & Pan D β-Catenin destruction complex-independent regulation of Hippo–YAP signaling by APC in intestinal tumorigenesis. Genes Dev. 29, 1493–1506 (2015). [PubMed: 26193883]
21. Kim HB et al. Prostaglandin E_2 activates YAP and a positive-signaling loop to promote colon regeneration after colitis but also carcinogenesis in mice. Gastroenterology 152, 616–630 (2017). [PubMed: 27864128]
22. Yu FX et al. Regulation of the Hippo–YAP pathway by G-protein-coupled receptor signaling. Cell 150, 780–791 (2012). [PubMed: 22863277]
23. Liu-Chittenden Y et al. Genetic and pharmacological disruption of the TEAD–YAP complex suppresses the oncogenic activity of YAP. Genes Dev. 26, 1300–1305 (2012). [PubMed: 22677547]
24. Mills JC & Sansom OJ Reserve stem cells: differentiated cells reprogram to fuel repair, metaplasia, and neoplasia in the adult gastrointestinal tract. Sci. Signal. 8, re8 (2015).
25. Nusse YM et al. Parasitic helminths induce fetal-like reversion in the intestinal stem cell niche. Nature 559, 109–113 (2018). [PubMed: 29950724]
26. Huyghe JR et al. Discovery of common and rare genetic risk variants for colorectal cancer. Nat. Genet. 51, 76–87 (2019). [PubMed: 30510241]
27. Ishikawa TO & Herschman HR Conditional knockout mouse for tissue-specific disruption of the cyclooxygenase-2 (Cox-2) gene. Genesis 44, 143–149 (2006). [PubMed: 16496341]
28. Armaka M et al. Mesenchymal cell targeting by TNF as a common pathogenic principle in chronic inflammatory joint and intestinal diseases. J. Exp. Med. 205, 331–337 (2008). [PubMed: 18250193]
29. Muzumdar MD, Tasic B, Miyamichi K, Li L & Luo L A global double-fluorescent Cre reporter mouse. Genesis 45, 593–605 (2007). [PubMed: 17868096]
30. Moser AR, Pitot HC & Dove WF A dominant mutation that predisposes to multiple intestinal neoplasia in the mouse. Science 247, 322–324 (1990). [PubMed: 2296722]
31. Schneider A et al. Generation of a conditional allele of the mouse prostaglandin EP4 receptor. Genesis 40, 7–14 (2004). [PubMed: 15354288]
32. Zhang N et al. The Merlin/NF2 tumor suppressor functions through the YAP oncoprotein to regulate tissue homeostasis in mammals. Dev. Cell 19, 27–38 (2010). [PubMed: 20643348]
33. Madison BB et al. Cis elements of the villin gene control expression in restricted domains of the vertical (crypt) and horizontal (duodenum, cecum) axes of the intestine. J. Biol. Chem. 277, 33275–33283 (2002). [PubMed: 12065599]
34. Barker N et al. Identification of stem cells in small intestine and colon by marker gene Lgr5. Nature 449, 1003–1007 (2007). [PubMed: 17934449]
35. Madisen L et al. A robust and high-throughput Cre reporting and characterization system for the whole mouse brain. Nat. Neurosci. 13, 133–140 (2010). [PubMed: 20023653]
36. Roulis M et al. Intestinal myofibroblast-specific Tpl2–Cox-2–PGE2 pathway links innate sensing to epithelial homeostasis. Proc. Natl Acad. Sci. USA 111, E4658–E4667 (2014). [PubMed: 25316791]

37. Masoodi M & Nicolaou A Lipidomic analysis of twenty-seven prostanoids and isoprostanes by liquid chromatography/electrospray tandem mass spectrometry. Rapid Commun. Mass Spectrom. 20, 3023–3029 (2006). [PubMed: 16986207]

38. Macosko EZ et al. Highly parallel genome-wide expression profiling of individual cells using nanoliter droplets. Cell 161, 1202–1214 (2015). [PubMed: 26000488]

39. Shekhar K et al. Comprehensive classification of retinal bipolar neurons by single-cell transcriptomics. Cell 166, 1308–1323 (2016). [PubMed: 27565351]

40. Linderman GC, Zhao J & Kluger Y Zero-preserving imputation of scRNA-seq data using low-rank approximation. Preprint at bioRxiv 10.1101/397588 (2018).

41. van der Maaten L & Hinton G Viualizing data using t-SNE. J. Mach. Learn. Res. 9, 2579–2605 (2008).

42. Ester M, Kriegel H-P, Sander J & Xu X A density-based algorithm for discovering clusters in large spatial databases with noise. KDD 96, 226–231 (1996).

43. Hänzelmann S, Castelo R & Guinney J GSVA: gene set variation analysis for microarray and RNA-seq data. BMC Bioinformatics 14, 7 (2013). [PubMed: 23323831]

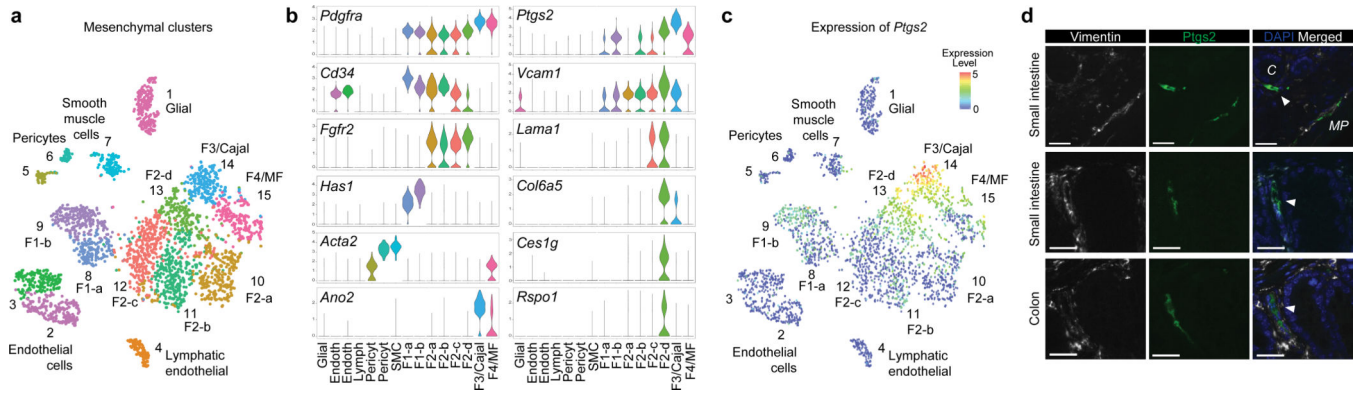

Fig. 1 |. Single-cell analyses of the intestinal mesenchyme reveal a rare fibroblast population that expresses *Ptgs2* and its protein product Cox-2, located under the crypts.

a–**c**, Single-cell RNA-seq of 3,179 mesenchymal cells from the normal mouse colon. **a**, *t*-distributed stochastic neighbour embedding (*t*-SNE) plot with clustering results. F, fibroblasts. MF, myofibroblasts. **b**, Violin plots showing the entire range of mesenchymal marker gene expression levels per single cell in each cluster. SMC, smooth muscle cells. **c**, *Ptgs2* expression levels per single cell visualized by *t*-SNE plot. **d**, Immunostaining for Cox-2 and Vimentin in the normal mouse ileum and colon. Cox-2-expressing fibroblasts are located under the crypt (C) epithelium (white arrowheads) and in the muscularis propria (MP). Results are representative of three independent experiments. Scale bars, 20 μm.

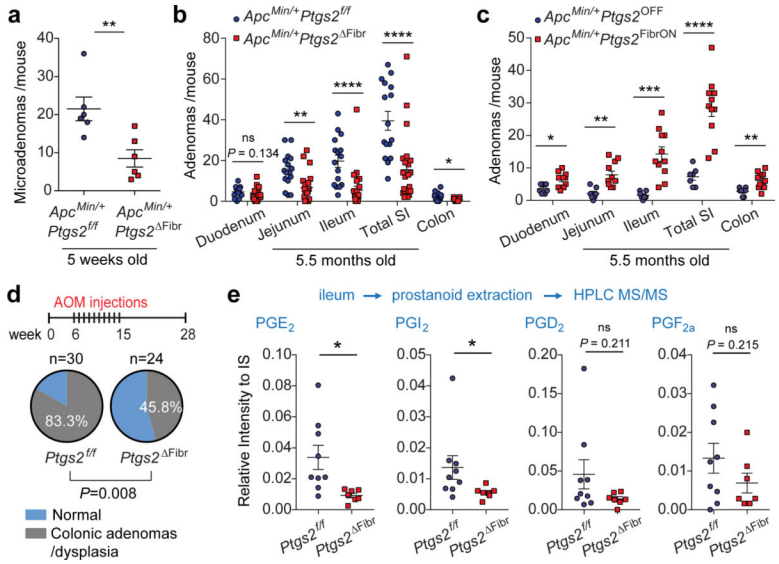

Fig. 2 |. *Ptgs2*-expressing fibroblasts drive tumour initiation by secreting PGE_2 in the crypt microenvironment.

a, Number of β-catenin$^+$ microadenomas in two sections of the small intestine (SI) of 5-week-old $Apc^{Min/+}Ptgs2^{f/f}$ ($n = 6$) and $Apc^{Min/+}Ptgs2^{\Delta Fibr}$ ($n = 6$) mice. Two-tailed *t*-test. **b**, Number of macroscopic adenomas in 5.5-month-old $Apc^{Min/+}Ptgs2^{f/f}$ ($n = 16$) and $Apc^{Min/+}Ptgs2^{\Delta Fibr}$ ($n = 23$) mice. Two-tailed Mann–Whitney test. **c**, Number of macroscopic adenomas in 5.5-month-old $Apc^{Min/+}Ptgs2^{OFF}$ ($n = 7$) mice in which *Ptgs2* expression is blocked, and $Apc^{Min/+}Ptgs2^{FibrON}$ ($n = 11$) littermates in which *Ptgs2* is exclusively expressed in fibroblasts (Extended Data Fig. 3i). Two-tailed Mann–Whitney test (duodenum), *t*-test (jejunum and colon), Welch's *t*-test (ileum and total small intestine). **d**, Incidence of dysplasia and microadenoma development in the colon of $Ptgs2^{f/f}$ ($n = 30$) and $Ptgs2^{\Delta Fibr}$ ($n = 24$) mice treated with 10 weekly injections of azoxymethane (AOM). Two-sided Fisher's exact test. **e**, HPLC–MS/MS analysis of prostanoids in the ileum of littermate $Ptgs2^{f/f}$ ($n = 9$) and $Ptgs2^{\Delta Fibr}$ ($n = 7$) mice. IS, internal standard. Two-tailed *t*-test (PGE_2 and PGF_{2a}) and Mann–Whitney test (PGI_2 and PGD_2). Data are mean ± s.e.m. NS, non-significant; $*P < 0.05$; $**P < 0.01$; $***P < 0.001$; $****P < 0.0001$.

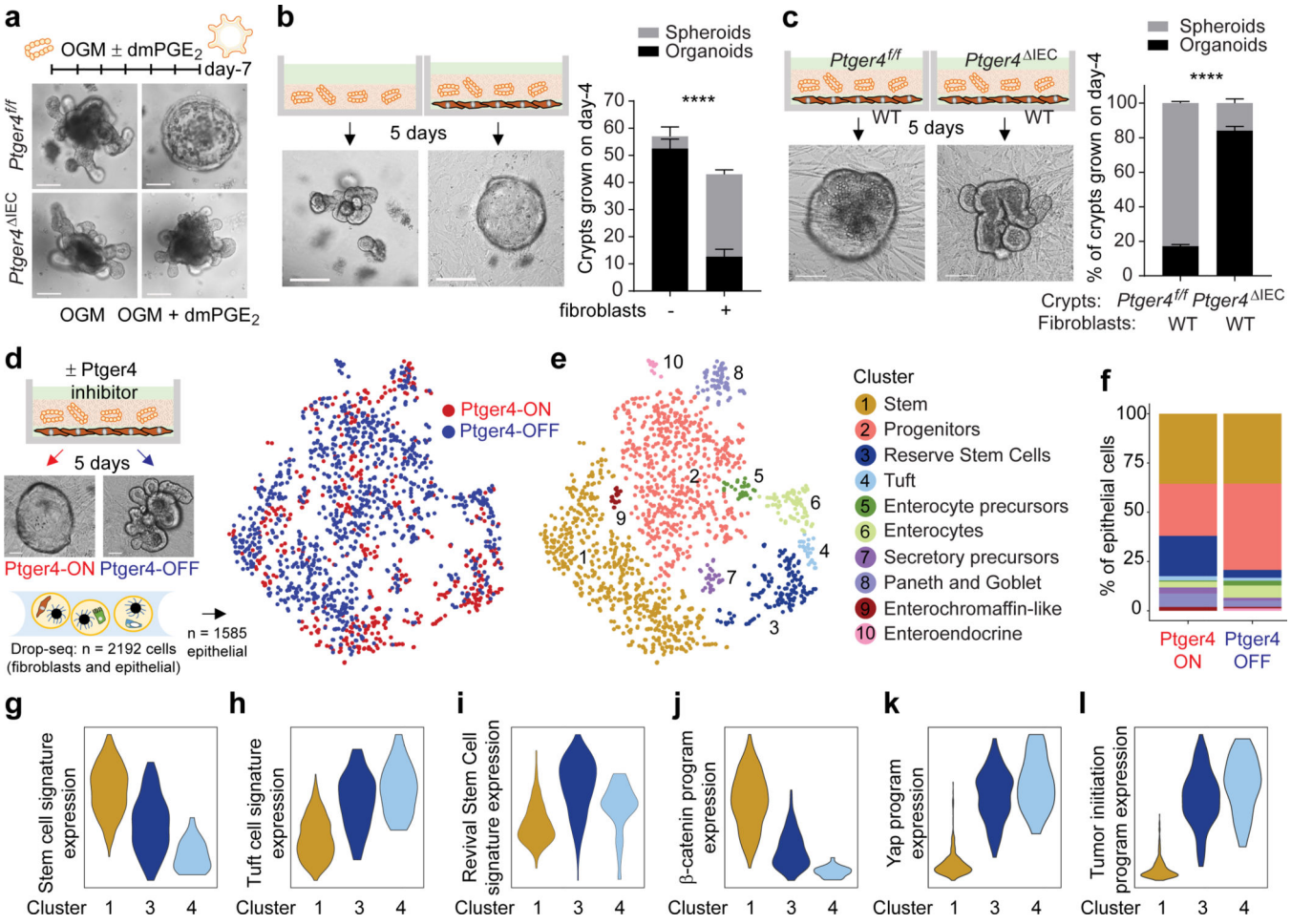

Fig. 3 |. Fibroblast-derived PGE_2 drives the expansion of RSCs with a Yap-driven pro-tumorigenic program via receptor Ptger4.

a, Indicative 3D cultures of crypts isolated from *Ptger4*$^{f/f}$ and *Ptger4*$^{\Delta IEC}$ mice grown with OGM or OGM supplemented with 0.1 μM $dmPGE_2$. Scale bar, 100 μm. **b**, Normal crypts were cultured as 3D organoids in OGM ($n = 2$) or in co-cultures with primary mouse intestinal fibroblasts ($n = 3$). The absolute numbers of organoids or spheroids per 3D culture are shown. Results are representative of five independent experiments. Scale bar, 200 μm. **c**, Crypts isolated from *Ptger4*$^{f/f}$ and *Ptger4*$^{\Delta IEC}$ mice were grown in co-cultures with wild-type (WT) primary mouse intestinal fibroblasts ($n = 3$ per genotype). The percentage of organoids and spheroids grown per 3D culture is shown. Results are representative of two independent experiments. Scale bar, 100 μm. In **b**, **c**, data are mean ± s.e.m.; two-way ANOVA, ****$P <$ 0.0001. **d**–**l**, Single-cell RNA-seq of intestinal crypt–fibroblast co-cultures grown in OGM with 10 μM Ptger4 inhibitor (Ptger4-OFF) or DMSO (Ptger4-ON). Analyses are shown for 1,585 epithelial cells. **d**, *t*-SNE plot indicating epithelial cells from co-cultures with Ptger4-ON or Ptger4-OFF. **e**, *t*-SNE plot with clustering results. **f**, Proportion of each epithelial cluster among total epithelial cells in co-cultures with Ptger4-ON or Ptger4-OFF. **g**–**l**, Violin plots showing the entire range of metagene expression levels per single cell per cluster for the signatures/transcriptional programs of stem cells[15] (**g**), tuft cells[15] (**h**), RSCs[16] (**i**), β-catenin (**j**), Yap (**k**) and early (non-tumour) *Apc*$^{min/+}$ tumorigenesis (**l**).

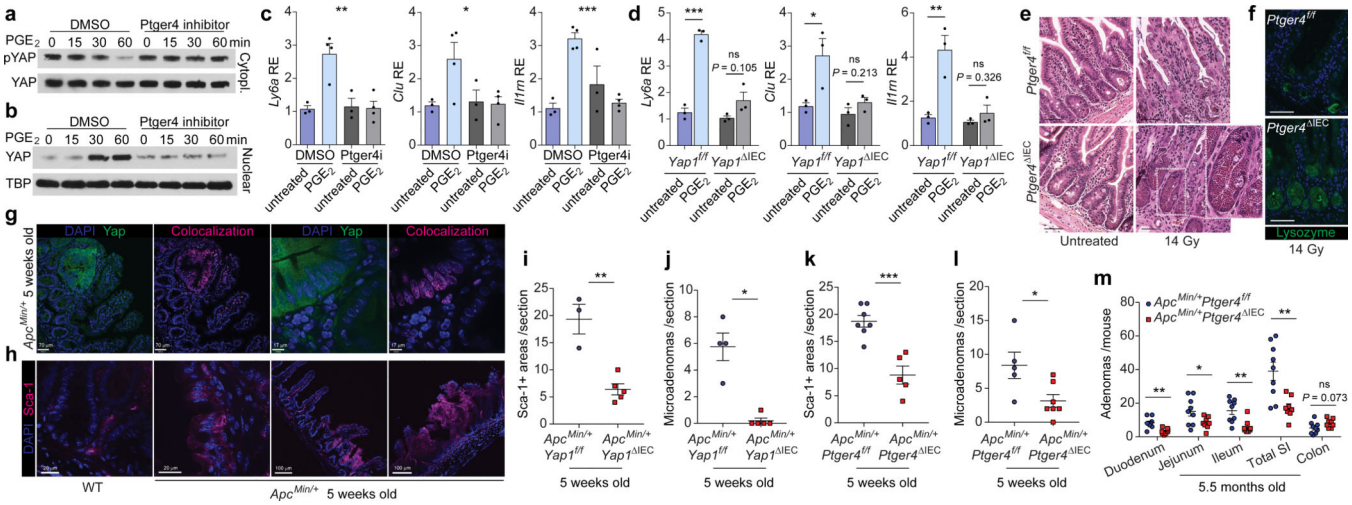

Fig. 4 |. Epithelial Ptger4 induces Yap nuclear translocation, mediates RSC mobilization and drives tumour initiation.

a, **b**, Wild-type organoids pretreated with or without 10 μM Ptger4 inhibitor were stimulated with 0.1 μM dmPGE$_2$.Western blots for phosphorylated Yap Ser127 (pYap) and total Yap in cytoplasmic lysates (**a**), Yap and TBP in nuclear lysates (**b**). Results are representative of two experiments. **c**, **d**, Relative expression of Yap target genes[18]. **c**, Wild-type organoids treated with 10 μM Ptger4 inhibitor and 0.1 μM dmPGE$_2$ for 13 h. $n = 3$ to 4 cultures per condition. One-way ANOVA. **d**, *Yap1*$^{\Delta IEC}$ and *Yap1*$^{f/f}$ organoids treated with 0.1 μM dmPGE$_2$ for 13 h. Three cultures per genotype per condition. Two-tailed *t*-test. **e**, **f**, *Ptger4*$^{f/f}$ ($n = 3$) and *Ptger4*$^{\Delta IEC}$ ($n = 3$) mice received 14 Gy of abdominal irradiation. On day 3, the ileum was analysed by haematoxylin and eosin staining (**e**) and immunostaining for lysozyme (**f**). Results are representative of three independent experiments. Scale bars, 50 μm. **g**, Immunostaining for Yap in the small intestine of five-week-old wild-type and *Apc*$^{Min/+}$ mice. Nuclear Yap is evaluated on the basis of colocalization with DAPI. Results are indicative of at least eight microadenomas. **h**, Immunostaining for Sca-1 in the small intestine of five-week-old wild-type and *Apc*$^{Min/+}$ mice. Results are representative of two independent experiments. **i**, **k**, Quantification of areas of the small intestine with expansion of Sca-1$^+$ epithelial cells in *Apc*$^{Min/+}$*Yap1*$^{f/f}$ ($n = 3$) and *Apc*$^{Min/+}$*Yap1*$^{\Delta IEC}$ ($n = 5$) mice (**i**), and *Apc*$^{Min/+}$*Ptger4*$^{f/f}$ ($n = 7$), *Apc*$^{Min/+}$*Ptger4*$^{\Delta IEC}$ ($n = 5$) mice (**k**). Two-tailed *t*-test. **j**, **l**, Number of BrdU$^+$ microadenomas per small-intestinal section of *Apc*$^{Min/+}$*Yap1*$^{f/f}$ ($n = 4$) and *Apc*$^{Min/+}$*Yap1*$^{\Delta IEC}$ ($n = 5$) mice (**j**), and *Apc*$^{Min/+}$*Ptger4*$^{f/f}$ ($n = 5$) and *Apc*$^{Min/+}$*Ptger4*$^{\Delta IEC}$ ($n = 7$) mice (**l**). Two-tailed Mann–Whitney test (**j**); two-tailed *t*-test (**l**). **m**, Number of macroscopic adenomas in 5.5-month-old *Apc*$^{Min/+}$*Ptger4*$^{f/f}$ ($n = 9$) and *Apc*$^{Min/+}$*Ptger4*$^{\Delta IEC}$ ($n = 8$) mice. Two-tailed *t*-test (duodenum and colon); Welch's *t*-test (jejunum and total small intestine); Mann–Whitney test (ileum). Data are mean ± s.e.m.